

# Chemical abundances in the globular clusters NGC 5024 and NGC 5466 from optical\* and infrared spectroscopy

M.P. Lamb<sup>1,5</sup>†, K.A. Venn<sup>1</sup>, M.D. Shetrone<sup>2</sup>, C.M Sakari<sup>1,3</sup>, and B.J. Pritzl<sup>4</sup>

<sup>1</sup>*Department of Physics and Astronomy, University of Victoria, Victoria, British Columbia, V8W 3P2, Canada*

<sup>2</sup>*Mcdonald Observatory, University of Texas at Austin, HC75 Box 1337-MCD, Fort Davis, TX 79734, USA*

<sup>3</sup>*Department of Astronomy, University of Washington Seattle, Seattle, WA 98195, USA*

<sup>4</sup>*University of Wisconsin Oshkosh, Oshkosh, WI 54901, USA*

<sup>5</sup>*NRC Herzberg Institute of Astrophysics, 5071 West Saanich Road, Victoria, BC V9E 2E7, Canada*

24 May 2021

## ABSTRACT

Detailed chemical abundances for five stars in two Galactic globular clusters, NGC 5466 and NGC 5024, are presented from high resolution optical (from the Hobby-Eberley Telescope) and infrared spectra (from the SDSS-III APOGEE survey). We find  $[\text{Fe}/\text{H}] = -1.97 \pm 0.13$  dex for NGC 5466, and  $[\text{Fe}/\text{H}] = -2.06 \pm 0.13$  dex for NGC 5024, and the typical abundance pattern for globular clusters for the remaining elements, e.g., both show evidence for mixing in their light element abundance ratios (C, N), and AGB contributions in their heavy element abundances (Y, Ba, and Eu). These clusters were selected to examine chemical trends that may correlate them with the Sgr dwarf galaxy remnant, but at these low metallicities no obvious differences from the Galactic abundance pattern are found. Regardless, we compare our results from the optical and infrared analyses to find that oxygen and silicon abundances determined from the infrared spectral lines are in better agreement with the other alpha-element ratios and with smaller random errors.

**Key words:** stars: abundances – techniques: spectroscopic – globular clusters: individual(NGC 5024) – globular clusters: individual(NGC 5466).

## 1 INTRODUCTION

The discovery of the accretion of globular clusters from the Sagittarius dwarf galaxy (Da Costa & Armandroff 1995), has led to the question as to how many globular clusters have been captured by the Milky Way. Multiple studies have looked at the globular cluster systems of the Milky Way to derive an age-metallicity relationship and have come to different conclusions as to which clusters have likely been accreted (Forbes & Bridges 2010; Mackey & van den Bergh 2005; Leaman et al. 2013; Dotter et al. 2011). The question is still open as to which type of clusters are accreted and which form in situ; and furthermore what the fraction of each type is within the Milky Way.

Globular clusters (GC) formed in dwarf galaxies may differ from those found in the Galactic halo, depending on

their age and metallicity. Dwarf galaxies show a wide variety of star formation histories (Weisz et al. 2014; Hidalgo et al. 2014, 2011) that are predicted to lead to variations in their metallicity distribution functions and chemical abundances. It has also been suggested these variations could be attributed to differences in the IMFs of these galaxies (McWilliam et al. 2013). If the IMFs are the root cause of these differences then this would also lead to differences in the age-metallicity relationship, which is observed by both Forbes & Bridges (2010) and Leaman et al. (2013). From observations, field stars in dwarf galaxies do exhibit different abundance ratios from Milky Way (MW) field stars, e.g., lower  $[\alpha/\text{Fe}]$  ratios and variations in neutron capture element ratios at intermediate metallicities. However these typically do not show up until  $[\text{Fe}/\text{H}] \sim -1.5$  (Shetrone et al. 1998, 2001, 2003; Venn et al. 2004; Tolstoy et al. 2009; Okamoto et al. 2009; Frebel 2010b). At metallicities below  $[\text{Fe}/\text{H}] = -1.5$  the abundance variations between field and GC stars become less pronounced in dwarfs and the MW (Letarte et al. 2010; Hill et al. 2000; Carretta et al. 2010; Pritzl et al. 2005); a good example of this is M54, located at the heart of the Sagittarius (Sgr) dwarf accretion remnant. M54 has a much lower metallicity than the Sgr field stars

\* Based on observations obtained with the Hobby-Eberly Telescope, which is a joint project of the University of Texas at Austin, the Pennsylvania State University, Stanford University, Ludwig-Maximilians-Universitt Munchen, and Georg-August-Universitt Gttingen.  
† E-mail: masen@uvic.ca

(e.g., Carretta et al. 2010) and the  $[\alpha/\text{Fe}]$  ratios resemble the field stars in the MW halo and its detailed chemical abundance ratios resemble the patterns seen in other globular cluster systems (e.g., the Na-O anti-correlation; Carretta et al. 2009). Therefore, other than its physical association with the Sgr remnant, M54 does not stand out from other GCs in terms of its chemical abundance patterns, similar to the metal-poor GCs Terzan 8 and Arp 2 (both also kinematically and spatially associated with the Sgr stream Mottini et al. 2008). On the other hand, Hodge 11 in the LMC at  $[\text{Fe}/\text{H}] = -2.0$  does have lower  $[\alpha/\text{Fe}]$  than MW field and GC stars (Mateluna et al. 2012); and Ruprecht 106 has an anomalously low  $[\alpha/\text{Fe}]$  ratio for a MW GC (Villanova et al. 2013).

Two metal-poor clusters that have been associated with the Sgr stream are NGC 5024 (M53) and NGC 5466 (Bellazzini et al. 2003; Martínez-Delgado et al. 2004). Both of these clusters are more metal-poor than M54 (each at  $[\text{Fe}/\text{H}] \sim -2$ , Harris 1996), which means that detailed chemistry could be inconclusive as to their origins in the Sgr dwarf galaxy. We have opted to study the chemistry in these GCs regardless though because (1) there are few published chemistries for these clusters and (2) they are both associated with other interesting dynamical structures. NGC 5466 has a large tidal tail (Grillmair & Johnson 2006). However it appears to have no association with the Sgr stream, and knowing the chemistry of this GC can help identify members in the tidal feature. It is also worth noting that NGC 5466 has a retrograde orbit, suggestive of an extragalactic origin (Allen et al. 2006; Forbes & Bridges 2010). NGC 5024 may be linked by a stellar bridge to NGC 5053 (Chun et al. 2010; Bellazzini et al. 2003), although no bridge was seen by Jordi & Grebel (2010), and detailed chemical abundances of stars in these two clusters can be used to study if their formation was coeval.

Detailed chemical abundances have been determined for a few stars in these clusters; one star in NGC 5024 and two stars in NGC 5466 by Pilachowski et al. (1983) (at lower resolution and S/N than discussed in this paper, see Section 2.1), and one anomalous cepheid in NGC 5466 by McCarthy & Nemeč (1997). Iron abundances for several stars in NGC 5024 have also been estimated from photometry by Dékány & Kovács (2009). All of these analyses confirm the metallicities of  $[\text{Fe}/\text{H}] \sim -2$  dex (Harris 1996; 2010). Carbon abundances have been derived from CN and CH band strengths for over a dozen stars in both NGC 5024 and NGC 5466 from Martell et al. (2008) and Shetrone et al. (2010), respectively. In both clusters, large variations in the  $[\text{C}/\text{Fe}]$  ratios are found, typical of stars that have undergone deep mixing on the red giant branch.

In this paper, we determine the chemical composition of individual stars in each GC. Abundances are determined from both optical and infrared spectroscopic data. This larger wavelength coverage allows us to determine the abundances of more spectral lines and more elements (e.g., CN, CO, OH, Si, and Al are ubiquitous in the IR yet rare in the optical). We also compare the accuracy of the abundance results between the two wavelength regions (similar to Smith et al. 2013).

## 2 OBSERVATIONS AND DATA REDUCTION

### 2.1 Observing Program

Five red giant branch (RGB) stars have been selected in the outer regions of two globular clusters, NGC 5024 and NGC 5466, for detailed spectral analyses. The locations of these objects are shown in Fig. 1 and their fundamental properties are listed in Table 1. Targets were chosen based on their V magnitudes, and V-I colours from the Stetson database (Stetson 2000). Foreground contamination is minimal.

Optical spectra were gathered with the High Resolution Spectrograph (HRS, Tull 1998) on the HET<sup>1</sup>. The HRS was configured at resolution  $R = 30,000$  with  $2 \times 2$  pixel binning using the 2 arcsecond fibre. The HRS splits the incoming beam onto two CCD chips, from which the spectral regions 6000 - 7000 Å (red chip) and 4800 - 5900 Å (blue chip) were extracted for this work. Two standard stars were also observed, RGB stars with previously published spectral analyses in each of the globular clusters M3 and M13. The signal to noise (S/N) for these seven targets ranged from 40 - 85 (see Table 1).

IR spectra for four of the five targets in NGC 5466 and NGC 5024 are available in the APOGEE DR10 release<sup>2</sup>. APOGEE provides H-band spectra, ranging from 15000-17000 Å at a resolution  $R \sim 20,000$  with  $S/N \geq 100$ . These spectra expand the analysis of our main science targets to features at longer wavelengths. We have not analysed the APOGEE spectra of our M3 and M13 standard stars since there are no published results of their infrared spectral features for a comparison.

### 2.2 Optical Data Reduction

The HET-HRS data were reduced using standard IRAF<sup>3</sup> packages. Some data was taken over multiple nights. Therefore data was reduced per night and coadded in those circumstances (see Table 1).

For each science observation, bias images (5), flat field images (5), a wavelength calibration, and a telluric standard star (a rapidly-rotating hot star) were also obtained. A medianed bias was subtracted from the red CCD images, but not the blue CCD images at the suggestion of the HET data reduction manuals<sup>4</sup> as this CCD is very clean and bias subtracting can add noise. Three science exposures from 2005 were taken with an older red CCD that suffered from hot pixels and bad columns - these exposures were corrected in IRAF (using *fixpix*). Images were divided by a medianed flat field, and scattered light was removed before aperture extraction. Spectra were extracted with variance weighting (to reduce cosmic ray contamination), and wavelength calibrated using a standard thorium-argon lamp. The telluric

<sup>1</sup> Observing time was allocated through NOAO program number 05 A-330, via the predecessor of the TSIP program, i.e., the NSF Facilities Instrumentation Program

<sup>2</sup> <https://www.sdss3.org/dr10/>

<sup>3</sup> IRAF (Image Reduction and Analysis Facility) is distributed by the National Optical Astronomy Observatory, which is operated by the Association of Universities for Research in Astronomy, Inc., under cooperative agreement with the National Science Foundation.

<sup>4</sup> <http://hydra.as.utexas.edu/?a=help&h=29#HRS>

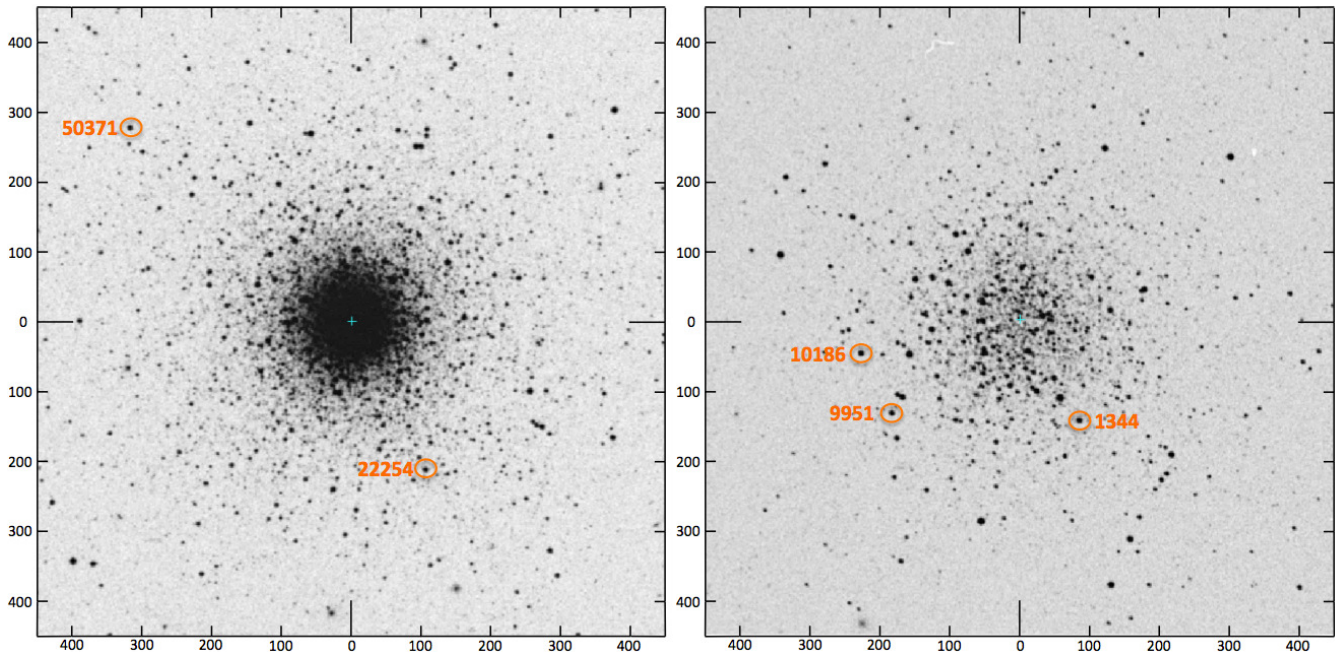


**Figure 1.** Positions of our science targets in NGC 5024 (left) and NGC 5466 (right). Axes are in arc seconds from the cluster centre (the centre is noted by the cyan cross in each image). North is up and East is left. Images taken from the SDSS survey.

**Table 1.** The sample of stars observed in the optical with the HET

Star	R.A. (J2000)	Dec. (J2000)	Date Obs.	Exp. Time (s) <sup>a</sup>	Red S/N @6250Å	Blue S/N @5500Å	$V_{hel.}$ (km/s)
NGC 5024-22254	13 12 47.94	+18 06 32.1	May 2005	2700(1)	50	40	-57.57 ± 0.50
NGC 5024-50371	13 13 17.36	+18 14 46.4	March 2007	3387(1)	75	55	-62.69 ± 0.24
NGC 5466-9951	14 05 41.08	+28 29 48.2	June 2005	6350(2)	60	55	126.53 ± 1.10
NGC 5466-1344	14 05 20.73	+28 29 42.0	June 2006	6600(3)	70	60	129.29 ± 0.81
NGC 5466-10186	14 05 44.53	+28 31 13.5	July 2006	3300(1)	70	60	107.33 ± 0.48
M3-C41303-2217	13 41 30.30	+28 29 42.0	March 2008	3000(1)	50	40	-145.25 ± 0.37
M13-III-18	16 41 24.64	+36 25 45.0	March 2008	3000(1)	85	75	-233.64 ± 0.23

<sup>a</sup> Total exposure time is listed, including the number of nights that observations were taken.

standards were reduced by the same methods, and divided into the science spectra to remove atmospheric features. The sky fibre on the HRS was not used because our science targets are quite bright.

Samples of the final spectra are shown in Fig. 2. Radial velocities were calculated using the IRAF task *fxcor*, and cross-correlating the heliocentric-corrected spectrum of Arcturus (Hinkle & Wallace 1995). These values are listed in Table 1. The velocities in NGC 5466 are in excellent agreement with those calculated per star by Shetrone et al. (2010). Thus this cluster shows a significant dispersion (Shetrone et al. 2012 finds a velocity dispersion of  $\sim 17$  km/s from 67 stars).

Post-pipeline processed APOGEE spectra are available in the SDSS DR10 database, where they have been reduced and coadded when multiple exposures were taken, and then continuum normalized. We took an additional step and shifted these spectra from the vacuum rest frame to the air rest frame.

### 3 EQUIVALENT WIDTH ANALYSIS OF OPTICAL SPECTRA

Optical abundances are determined from an equivalent width (EW) analysis. All equivalent widths were initially measured using DAOSPEC (Stetson & Pancino 2008)<sup>5</sup>. The atomic lines used with DAOSPEC are comprised of a list taken from several sources: Shetrone et al. (2003), Cayrel et al. (2003), Aoki et al. (2007), Cohen et al. (2008), Letarte et al. (2009), Tafelmeyer et al. (2010), Frebel et al. (2010a), and Venn et al. (2012). Discrepancies between DAOSPEC and *splot* occur for lines with EWs greater than 100 mÅ; the IRAF measurements were adopted for lines  $> 100$  mÅ. Lines were also examined by eye for unrecognized blends or

<sup>5</sup> DAOSPEC is a program that is capable of measuring equivalent widths and radial velocities of spectra. It was written by P.B. Stetson for the Dominion Astrophysical Observatory, National Research Council, Canada.

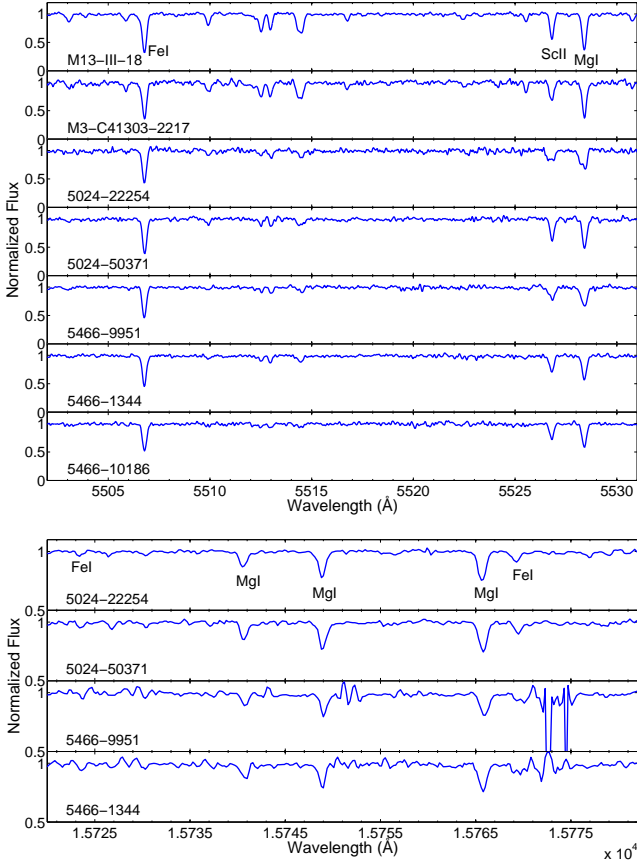


**Figure 2.** Sample spectral regions in the optical (blue chip, top), and infrared (bottom) showing magnesium, scandium, and iron lines that were used in the abundance analysis.

other mismasurements (i.e. contaminated with noise spikes, etc.), using the spectrum of Arcturus and the Sun as references. Lines with EWs > 200 mÅ were not analysed since they tend to be very sensitive to small uncertainties in microturbulence and other stellar atmosphere effects.

### 3.1 $\Delta EW$

The uncertainty in EW measurements can be estimated from the revised Cayrel formula (Battaglia et al. 2008; Cayrel 1989),

$$\Delta(EW) \sim \frac{\sqrt{1.5 \cdot FWHM \cdot \Delta x}}{S/N} \quad (1)$$

where FWHM is the measured full width at half maximum of a particular line in Å,  $\Delta x$  is the dispersion of the spectra in Å/pixel (37.9 mÅ for the Blue chip and 50.89 mÅ for the Red), and S/N is the signal-to-noise measured in the wavelength region of the particular line being measured. For a stronger line (EW  $\sim$  100 mÅ) then  $\Delta(EW) = 2.7$  mÅ ( $\sim$  3% error) whereas weaker lines (EW  $\sim$  20 mÅ) yield a value closer to 10% error. Thus we conservatively adopt 10% as the uncertainty in EW measurements for each line.

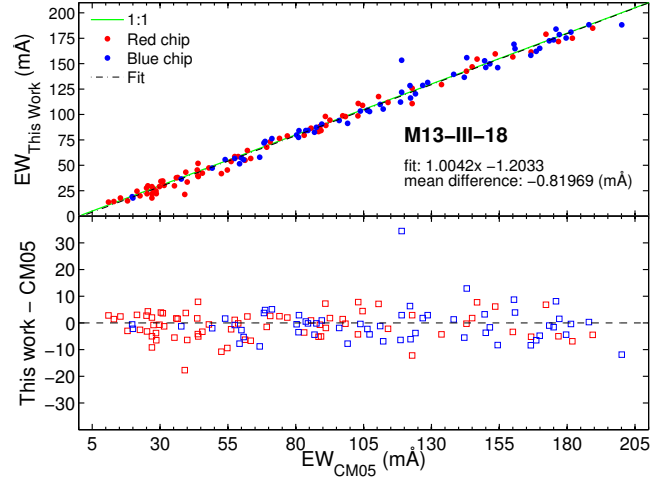


**Figure 3.** Measured equivalent widths with DAOSPEC vs. CM05 for M13.

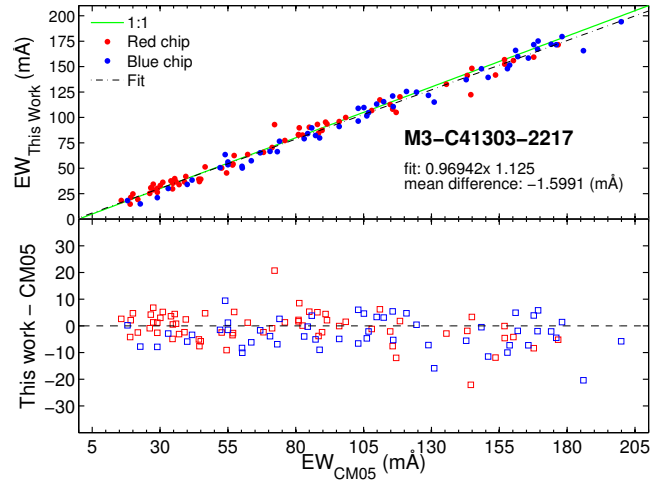


**Figure 4.** Measured equivalent widths with DAOSPEC vs. CM05 for M3.

### 3.2 EW Comparison with Standard Stars

To test the validity of the analysis procedure, two standard stars are analysed using the same method as the target stars: M3-C41303-2217 and M13-III-18. Figs 3 and 4 show a comparison of EW measurements (this work) compared with those from Cohen & Meléndez (2005, hereafter referred to as CM05). A mean difference (This Study - Literature) of  $-0.819$  mÅ ( $\sigma = 5.836$  mÅ) is found in M13-III-18 (from 127 lines) and a difference of  $-1.599$  mÅ ( $\sigma = 5.967$  mÅ) is found for M3-C41303-2217 (from 115 lines). This agreement is reasonable and these measurement methods are applied to the new targets in NGC 5024 and NGC 5466.

## 4 MODEL ATMOSPHERE AND ABUNDANCE ANALYSIS OF OPTICAL DATA

The optical abundances are computed by using the radiative transfer code MOOG (Snedden 1973), which uses stellar model atmospheres and atomic data to synthesize spec-

**Table 2.** Equivalent Widths and Atomic Data

Ion	$\lambda$ (Å)	$\chi$ (eV)	$\log gf$	NGC 5024		NGC 5466			M3	M13
				22254 (mÅ)	50371 (mÅ)	1344 (mÅ)	9951 (mÅ)	10186 (mÅ)	C41303-2217 (mÅ)	III-18 (mÅ)
Fe I	5302.302	3.28	-0.880	78.4	94.9	83.4	78.5	75.5	109.0	123.7
Fe I	5307.370	1.61	-2.912	68.8	93.3	91.1	83.7	74.5	123.1	122.2
Fe I	5324.190	3.21	-0.100	123.3	123.9	111.8	123.8	111.5	158.4	158.2
Fe I	5339.930	3.27	-0.720	95.9	92.7	79.3	75.3	77.1	123.8	127.3
Fe I	5364.860	4.45	0.228	54.4	56.8	57.3	61.7	54.3	86.8	93.3
...										

\*Full table available online

tra. The new MARCS spherical models have been adapted (Gustafsson et al. 2008, 1975, also see Mészáros et al. 2012) assuming  $[\alpha/\text{Fe}]$  enhancement since the science targets and standard stars are relatively metal-poor ( $[\text{Fe}/\text{H}] < -1$  dex). This combination of spherical model atmospheres and MOOG’s plane parallel radiative transfer is appropriate for analyzing red giants (e.g. see Heiter & Eriksson 2006 and additional tests by Venn et al. 2012).

#### 4.1 Photometric Stellar parameters

The stellar parameter  $T_{\text{eff}}$  is computed using the infrared flux method (IRFM, described by Ramírez & Meléndez 2005), which requires precision photometry, reddening, distance modulus, metallicity, and stellar mass. Using this  $T_{\text{eff}}$  and an estimate of the stellar mass, the surface gravity can be determined.

Optical photometry comes from the Stetson database<sup>6</sup> and the infrared photometry comes from 2MASS (Skrutskie et al. 2006, see Table 3). Typical errors for both photometric sources are  $\sim 0.02$  mag. Reddening values are from the Harris catalogue; typical reddening errors are 10%. Distance moduli are from the Harris catalogue as determined from the horizontal branch magnitude (taken from Kopacki 2000 for NGC 5024 and from Fekadu et al. 2007 for NGC 5466). The uncertainty in the distance moduli are 0.1 mag. Input metallicities are taken from the literature: either from direct Fe measurements or from the average cluster metallicity (see Table 3). Assuming the RGB mass is roughly equivalent to the main sequence turnoff (MSTO) mass, an input stellar mass of  $0.8M_{\odot}$  is taken from the MSTO of the isochrone fits of NGC 5024/5466 (Dotter et al. 2010)<sup>7</sup>. The isochrone with the larger age uncertainty is NGC 5466 ( $\sigma = 0.75$  Gyr, reflecting a larger intrinsic scatter in its CMD), resulting in a maximum turnoff mass uncertainty of  $\Delta M_{\text{turnoff}} = 3\%$ .

<sup>6</sup> <http://www4.cadc-ccda.hia-ihp.nrc-cnrc.gc.ca/community/STETSON/standards/>

<sup>7</sup> the actual isochrones corresponding to the GC parameters in Dotter et al. (2010) can be downloaded from The Dartmouth Stellar Evolution Database (<http://stellar.dartmouth.edu/models/>) and manually searched for a turn-off mass.

#### 4.2 Spectroscopic Stellar Parameters

Stellar model atmospheres were interpolated from the grid of MARCS models using the initial parameters discussed in Section 4.1. These models were run with MOOG to compute initial line abundances from EW measurements. Revised values of  $T_{\text{eff}}$  and  $\log \epsilon(\text{Fe I})$ , and new microturbulence values were found.  $T_{\text{eff}}$  is adjusted in small increments to find the best fit to the Fe I line abundances when plotted against the excitation potential ( $\chi$ ). Simultaneously the microturbulence is adjusted such that there is no dependence between  $\log \epsilon(\text{Fe I})$  and the reduced EWs. This process is repeated until the final slopes in Fe I vs  $\chi$  and reduced EW were  $< 0.004$ . These spectroscopic parameters are listed in Table 4; in the case of  $T_{\text{eff}}$  the spectroscopic and photometric values agree within the errors. We refer the reader to Section 6.1 to demonstrate how these  $T_{\text{eff}}$  differences affect the derived stellar abundances (i.e. see Table 5). Also included in the table are the derived stellar parameters from the APOGEE Stellar Parameters and Chemical Abundance Pipeline (ASPCAP<sup>8</sup>, García Pérez et al. 2014, in preparation) for Fe, C and N.

#### 4.3 Stellar Parameter Uncertainties

The uncertainties in  $T_{\text{eff}}$  were found by assuming the derived individual Fe I line abundances are distributed randomly about the mean; thus the standard deviation ( $\sigma_{\text{Fe}}$ ) in the mean abundance measures the scatter in the data. If  $T_{\text{eff}}$  is adjusted such that the slope of the  $\log(\text{Fe})$  vs  $\chi$  spans  $\pm 1\sigma$  over the range in excitation potentials ( $\chi$ ), then  $\Delta T_{\text{eff}}$  is found to be  $\sim 100$  K for both standard stars, and this is adopted for the five science targets given the similarity in S/N and  $T_{\text{eff}}$  in our sample.

The  $\Delta v_t$  is found by allowing the slope  $\log \epsilon(\text{Fe I})$  vs. reduced EW to vary such that the range of  $\log \epsilon(\text{Fe I})$  values span  $1\sigma$  over the range of reduced EWs, similar to the method used to find  $\Delta T_{\text{eff}}$ . The  $\Delta v_t = 0.2 \text{ km s}^{-1}$  for both standard stars and is adopted for the five science targets.

Physical gravities are adopted from the IRFM, thus  $\log(g)$  depends on the distance to the star (or cluster), reddening,  $T_{\text{eff}}$  value, turn-off mass, and photometry; an estimate in the uncertainty of  $\log(g)$  is calculated by quantifying

<sup>8</sup> ASPCAP parameters were retrieved online at <http://data.sdss3.org/sas/dr10/apogee/spectro/redux/r3/fields.html>

**Table 3.** Photometric magnitudes and cluster properties

Star	Photometry <sup>a</sup>						Cluster parameters <sup>b,c</sup>		
	B	V	I	J	H	K	$(m - M)_V$	$E(B - V)$	Initial [Fe/H] (dex)
NGC 5024-22254	15.92	14.88	13.74	12.932	12.367	12.230	16.32	0.02	-2.10
NGC 5024-50371	15.64	14.56	13.35	12.574	11.973	11.878	16.32	0.02	-2.10
NGC 5466-9951	15.90	14.97	13.92	13.092	12.551	12.472	16.02	0.00	-1.98
NGC 5466-1344	15.67	14.67	13.58	12.725	12.153	12.056	16.02	0.00	-1.98
NGC 5466-10186	15.56	14.62	13.55	12.712	12.137	12.107	16.02	0.00	-1.98
M3-C41303-2217	14.86	13.75	12.58	11.698	11.118	10.969	15.07	0.01	-1.37±0.05
M13-III-18	13.94	12.74	11.51	10.601	9.928	9.830	14.33	0.02	-1.43±0.05

<sup>a</sup> All B, V, and I values taken from the Stetson database (Stetson 2000). All J, H, K values taken from the 2MASS survey.

<sup>b</sup> Distance modulus and reddening taken from Harris (1996; 2010)

<sup>c</sup> NGC 5024/5466 metallicity taken from the cluster metallicity itself (Harris 1996; 2010), M3 and M13 metallicities taken from CM05. These metallicities are used as input to determine initial stellar parameters.

**Table 4.** Derived Temperatures and Gravity

Star	This Study			CM05			ASPCAP <sup>a</sup> (APOGEE)			
	$T_{\text{eff}} (\pm 100 \text{ K})$ <sup>b</sup>		$\log(g)$ ( $\pm 0.2$ dex)	$v_t$ ( $\pm 0.2 \text{ km s}^{-1}$ )	$T_{\text{eff}}$ ( $\pm 75 \text{ K}$ )	$\log(g)$ ( $\pm 0.2$ dex)	$v_t$ ( $^{+0.4}_{-0.2} \text{ km s}^{-1}$ )	$T_{\text{eff}}$ (K)	$\log(g)$ (dex)	$v_t$ ( $\text{km s}^{-1}$ )
NGC 5024-22254	4511	4410	1.21	1.60	-	-	-	4409	1.37	1.83
NGC 5024-50371	4444	4425	1.06	1.80	-	-	-	4391	1.26	1.86
NGC 5466-9951	4595	4600	1.44	1.55	-	-	-	4512	1.75	1.71
NGC 5466-1344	4512	4499	1.27	1.40	-	-	-	4469	1.62	1.75
NGC 5466-10186	4571	4585	1.29	1.75	-	-	-	-	-	-
M3-C41303-2217	4379	4538	1.19	1.55	4436	1.20	1.60	4319	1.69	1.73
M13-III-18	4298	4397	1.02	1.75	4350	1.00	1.65	4498	2.25	1.56

<sup>a</sup> The uncertainties in these stellar parameters are very small and are therefore not included here.

<sup>b</sup> In this work we adopt spectroscopic  $T_{\text{eff}}$  as there are typically  $> 100$  Fe I lines available to constrain this parameter.

and propagating the errors in these parameters. After calculating  $\log(g)$  and varying these parameters by the errors described in this Section,  $\Delta \log(g) = 0.2$  dex (Assuming no covariance).

#### 4.4 Comparison of Stellar Parameters and Iron with the Standard Stars

To test the validity of this abundance analysis technique the procedure is applied to the standard stars in M3 and M13 using the model atmospheres and EWs of this work and comparing the Fe I abundance with CM05. The model atmosphere parameters of CM05 agree within the uncertainties of this work (see Table 4) and so the Fe comparison should yield consistent results. The derived M13 standard star [Fe/H] abundance from this work is  $-1.57 \pm 0.05$  whereas that of CM05 is  $-1.48 \pm 0.05$  and that of Sneden et al. (2004) is  $-1.50 \pm 0.05$  (after correcting both for different solar Fe abundances). The derived M3 standard star [Fe/H] abundance is  $-1.33 \pm 0.05$  whereas that of CM05 is

$-1.42 \pm 0.05$  (again correcting for different solar Fe abundances). We consider these results in good agreement (see Section 6.2 for an abundance comparison of all determined elements).

## 5 ABUNDANCE ANALYSIS OF INFRARED DATA

Chemical abundances in the IR are determined via spectrum synthesis, and not EWs. EWs are not practical in the IR due to the presence of molecular lines and blends across the entire spectrum. Synthetic spectra are calculated with MOOG using the model atmospheres described in Section 4 and the DR10 line list from Matthew Shetrone (Shetrone et al. in prep). A  $^{12}\text{C}/^{13}\text{C}$  ratio of 6 is adopted following Shetrone et al. (2010). However, at low metallicities the spectral features sensitive to this ratio (i.e.  $^{13}\text{C}^{16}\text{O}$ ) show no observable change when altering this ratio from 6 to 50. There is also no observable change in overall carbon abundance after al-

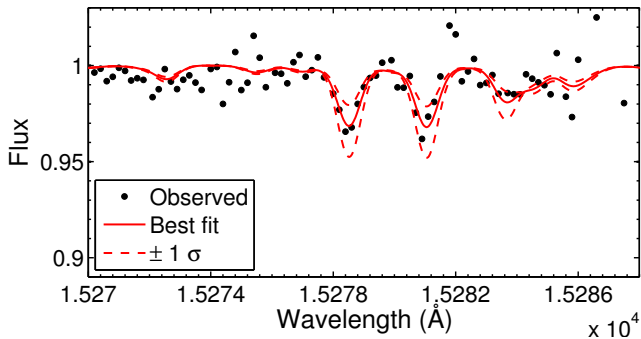


**Figure 5.** Example of a typical OH line measured in the infrared. This particular case is taken from NGC 5466 1344. The two dotted lines represent  $1\sigma$  abundance errors.

tering the ratio by this amount. Therefore the choice of this value over this range is not critical.

To find the iron abundance a preliminary selection of the most prominent iron lines ( $\sim 20$ ) is chosen over the spectral range 15100-16900 Å. The spectral region around each of these lines is synthesized with an iron abundance of zero to ensure the feature of interest vanishes and that no other elements or molecules contribute to the spectral line. The resulting sample of iron lines is typically reduced to  $\sim 12$ . The uncertainty for each measured iron line is determined by examining the residual between the synthetic and actual spectrum and finding the abundance which causes the residual to differ visually from the noise. The weighted average is computed for all of the individually examined iron lines and then set as the iron abundance for the synthesis of the rest of the elements. The error of the weighted mean is taken to be the final abundance uncertainty; this method is used to compute the uncertainties in all infrared abundance calculations except in the case of oxygen.

Oxygen has a slight dependance on the carbon abundance through CO formation. Therefore an initial carbon abundance is determined from the analysis of a single atomic C I line and several CO features, where carbon is much more sensitive than oxygen. With carbon fixed, the oxygen is then determined by synthesizing OH lines (see Fig. 5). The new oxygen abundance is fixed, and the carbon redetermined. This iteration is repeated until the carbon and oxygen abundances converge (typically two iterations). The oxygen uncertainty is first determined exactly as described above with iron, then it is added in quadrature to the value found from re-deriving the oxygen abundance after fluctuating carbon by its maximum error. Finally, nitrogen is found from CN regions using the final carbon abundance (see section 6.3.2 for the regions). The rest of the elements are then synthesized and their abundances determined. The final abundances are shown in Tables 7 and 8.

## 6 ABUNDANCE RESULTS

In this section, the abundance errors and standard star comparison are first addressed before comparing our results with the Galactic sample. The abundances with respect to Fe I from both wavelength regions are then compared with the literature in Section 6.3. The reported abundances are with

respect to solar, (Asplund et al. (2009)). Galactic comparison stars are taken from Venn et al. (2004), Frebel (2010b) (metal-poor stars), and Reddy et al. (2006) (thick disk stars) and comparison MW clusters are taken from Pritzl et al. (2005). Additional comparison stars for Cu and Zn are included from Mishenina et al. (2002). These comparison stars were chosen because their abundances were determined from high-resolution, high S/N spectra. For each element the specific spectral lines used to compute the abundances are discussed as well as any additional effects or corrections (i.e. hyperfine structure, NLTE, 3D effects, etc.). Hyperfine structure corrections are applied to the elements Sc, V, Mn, Co, Cu, Ba, and La; the isotopic data used to compute the corrections were collected from a variety of sources (Sc, V, Mn, and Co from Procheska et al. 2000, additional Mn from Booth et al. 1983, Cu from Biehl 1976, Ba from Lawler et al. 2001a, Eu and La from Lawler et al. 2001b), and the corrections are only found to be significant ( $>0.05$  dex) for V and Mn. The abundance errors and standard star comparisons are also discussed in this section.

### 6.1 Abundance Errors

The abundance errors are determined by combining intrinsic random errors in the sample with the errors associated with the stellar parameter uncertainties. The intrinsic errors in the sample are determined by computing the error in the mean (i.e.  $\sigma_X / \sqrt{N_X}$ ) except in the case where there were fewer than 5 lines of element X, in which case  $\sigma_{Fe} / \sqrt{N_X}$  is used. The abundance sensitivities due to stellar parameter uncertainties are calculated and summarized for a sample star (NGC 5024-22254) in Table 5. The final errors used with the Galactic comparison are determined by adding the random and stellar parameter uncertainties in quadrature (ignoring the covariant terms between temperature and microturbulence).

### 6.2 Standard Star Comparison

The standard star abundances are compared to CM05 in detail here. The EWs and stellar parameters between this work and CM05 are in good agreement, as summarized in Sections 3.2 and 4.4; thus the remaining elemental abundances are now compared. The standard star abundances are shown in Table 6 along with their random errors (the systematic errors are not included in the table to keep consistent with the similar table found in CM05); the average abundance difference ( $\pm\sigma$ ) between this work and CM05 is  $0.08 \pm 0.13$  and  $0.14 \pm 0.11$  for M3-C41303-2217 and M13-III-18 respectively which we consider good agreement. In the case where there are derived abundances for both the neutral and ionized species (except for the case of Fe), the weighted mean and error between the two is reported and compared with CM05. As opposed to the other elemental abundances, oxygen was determined with respect to Fe II in order to keep consistent with CM05.

For the M3 star most of the elements agree within the errors with the exception of Sc, V, Ni, and La (which lie within  $2\sigma$  of each other), of Ca ( $3\sigma$ ), and of Zn ( $4\sigma$ ). Snelten et al. (2004) find Sc to be  $-0.11$  dex lower than CM05 and we find also find Sc to be lower (by  $-0.16$  dex). The V abundance in this work has only 3 overlapping lines with CM05,

**Table 5.** Abundance Sensitivities for NGC 5024-22254

Species	$\Delta T_{\text{eff}}$ (+ 100K)	$\Delta \log g$ (+ 0.2 dex)	$\Delta v_t$ (+ 0.2 km/s)	Total <sup>a</sup>
Optical Data				
Fe I	-0.15	0.00	0.10	0.18
Fe II	0.06	-0.07	0.05	0.10
O I	-0.01	-0.04	0.01	0.04
Na I	-0.15	0.04	0.06	0.17
Mg I	-0.09	0.03	0.05	0.11
Al I	...	...	...	...
Si I	-0.01	-0.01	0.01	0.02
Ca I	-0.12	0.01	0.05	0.13
Sc II	0.01	-0.07	0.04	0.08
Ti I	-0.21	-0.01	0.05	0.22
Ti II	0.01	-0.06	0.08	0.10
V I	-0.21	-0.01	0.00	0.21
Cr I	-0.21	-0.01	0.08	0.22
Cr II	0.06	-0.06	0.03	0.09
Mn I	-0.15	0.02	0.08	0.17
Co I	-0.15	-0.01	0.01	0.15
Ni I	-0.13	-0.01	0.03	0.13
Cu I	-0.15	-0.01	0.01	0.01
Zn I	0.04	-0.03	0.04	0.06
Y II	-0.01	-0.07	0.10	0.10
Ba II	-0.05	-0.07	0.12	0.15
La II	-0.03	-0.08	0.01	0.09
Nd II	-0.03	-0.08	0.01	0.09
Eu II	...	...	...	...
Infrared Data				
Fe I	-0.07	0.01	0.00	0.07
C I	-0.01	-0.08	-0.05	0.09
N I	-0.15	0.09	0.06	0.18
O I	-0.18	0.00	-0.01	0.18
Mg I	-0.13	-0.01	-0.02	0.14
Al I	-0.11	-0.01	-0.04	0.12
Si I	-0.12	-0.03	-0.03	0.12
Ca I	-0.19	-0.10	-0.14	0.26
Ti I	-0.20	-0.05	-0.05	0.21

<sup>a</sup> All errors added in quadrature.

all with different  $\log(gf)$  values ( $\sim 0.05$  dex difference). The Ni abundances in this work are derived with  $\log(gf)$  values that are quite different than CM05, with all 8 of the overlapping lines showing differences up to 0.24 dex. La is derived from 2 lines in this work with similar EWs and  $\log(gf)$  values to CM05, and from one additional La line; after taking into account the differences in adopted solar values between this work and CM05 the La abundances agree within the errors. The M3 Ca abundance derived by Sneden et al. (2004) differs from CM05 by -0.13 dex, and the difference between this work and CM05 is also found to be lower (by -0.17 dex). There is only one common Zn line between this work and CM05; this line differs in both EW (by 17%) and in  $\log(gf)$  value (by 0.05 dex). The abundances of all elements mentioned here agree with CM05 when taking into account the systematic uncertainties, except in the case of Zn.

The M13 star also shows most elements agree within the errors with the exception of Na, and V (which lie within  $2\sigma$ ), of Ti, Ni, and Y ( $3\sigma$ ), and of Al, and Ca ( $4\sigma$ ). The Na abundances are computed from  $\log(gf)$  values that differ with CM05 by up to 0.05 dex and with excitation potentials that differ by up to 0.10 eV. V, Ni, Ca, and La derived

abundances share the same discrepancies discussed above with the M3 standard star. The Ti abundance is calculated from an average between TiI and TiII and in this work there are many more TiII lines than with CM05. The NLTE effects on TiI are well known and result in a lower TiI abundance compared to TiII (see Section 6.3.3), thus an average computed with more TiI lines than TiII (such as CM05) will inevitably ensure an overall lower Ti abundance as is shown for both standard stars. The Y abundance is derived from 4 lines, 3 of which are in common with CM05; the line that is not in common with CM05 yields a higher abundance by  $\sim 0.2$  dex. The Al abundance is derived from entirely different lines than CM05. For La there are only two out of four lines that overlap with CM05 and there are  $\sim 15\%$  discrepancies in EW for the common lines; furthermore if  $[La/Fe]$  is calculated using the solar values and Fe I parameters of CM05 then the La abundances agree. The comparisons of all elements mentioned here agree with CM05 when taking into account the systematic uncertainties, except in the case of Al as there is no reported systematic for this element in CM05.

Overall, the standard star comparison is within good agreement and we consider the methods used both here and with the target stars sound. The target star abundances are discussed in detail in the following section.

### 6.3 NGC 5024/5466 Stars

The final optical and infrared stellar abundances of the target stars are reported in Tables 7, 8, and 9, along with their random errors. For all of the comparisons with the Galactic sample (i.e. Figures 6-14), the abundance uncertainties reflect both the errors from the stellar parameters and random errors reported in the aforementioned Tables; the two errors are added in quadrature.

#### 6.3.1 Iron

The Fe I and Fe II abundance derived from the optical data are noticeably different in all stars, with differences ranging from 0.18 to 0.33 dex. It is well known that this is caused by NLTE effects on the Fe I lines, e.g., Bergemann et al. (2012); Lind et al. (2012) find that metal-poor RGB stars have Fe I abundances that are underestimated due to the overionization of iron by the radiation field (effects on Fe II are negligible). NLTE corrections<sup>9</sup> for NGC 5466-9951 (the star with the largest Fe I - Fe II discrepancy) are typically +0.1 dex for a sample of 24 lines. Assuming this is representative of our samples ( $>100$  Fe I lines per star in the optical), then we apply a global correction to our results (see Table 7). All elements from all ionization states are computed with respect to Fe I.

The iron abundances of the individual stars in both clusters agree with the cluster metallicities (see Table 3). We note the iron abundance spread in NGC 5466 is larger than the  $1\sigma$  measurement uncertainties, with one star at  $[Fe/H] = -2.19 \pm 0.05$  dex. We note if the global systematic error of  $[Fe/H]$  is considered than it can be seen to be

<sup>9</sup> Taken from the online database at <http://inspect-stars.net/>

**Table 7.** Derived abundances for NGC5466 and NGC5024: Fe I, C, N, O

Species <sup>d</sup>	Data source	Abundance ( $[X/Fe]$ ) <sup>a</sup> $\pm \sigma/\sqrt{N}$ (#) <sup>b,c</sup>				
		NGC5024-22254	NGC5024-50371	NGC5466-9951	NGC5466-1344	NGC5466-10186
Fe I	Optical	$-2.17 \pm 0.05$ (105)	$-2.15 \pm 0.05$ (114)	$-1.98 \pm 0.05$ (114)	$-2.02 \pm 0.05$ (114)	$-2.19 \pm 0.05$ (110)
	Infrared	$-2.19 \pm 0.07$ (12)	$-2.12 \pm 0.07$ (12)	$-2.00 \pm 0.07$ (16)	$-2.06 \pm 0.06$ (11)	...
	Ave. NLTE <sup>e</sup>	$-2.08 \pm 0.09$	$-2.04 \pm 0.09$	$-1.89 \pm 0.09$	$-1.94 \pm 0.08$	$-2.09 \pm 0.05$
	ASPCAP	$-2.07 \pm 0.01$	$-1.99 \pm 0.01$	$-1.89 \pm 0.05$	$-1.94 \pm 0.01$	...
C I	Optical	...	...	...	...	...
	Infrared	$-0.12 \pm 0.37$ (*)	$-0.28 \pm 0.33$ (*)	$-0.33 \pm 0.35$ (*)	$-0.20 \pm 0.20$ (*)	...
	ASPCAP	$-0.02 \pm 0.03$	$-0.15 \pm 0.05$	$-0.35 \pm 0.17$	$-0.17 \pm 0.08$	...
N I	Optical	...	...	...	...	...
	Infrared	$0.21 \pm 0.32$ (*)	$0.46 \pm 0.38$ (*)	$0.70 \pm 0.30$ (*)	$0.58 \pm 0.21$ (*)	...
	ASPCAP	$0.49 \pm 0.04$	$0.57 \pm 0.05$	$0.87 \pm 0.17$	$0.76 \pm 0.10$	...
O I	Optical	$0.74 \pm 0.18$ (1)	$0.89 \pm 0.17$ (1)	$0.38 \pm 0.19$ (1)	$0.59 \pm 0.16$ (1)	$< 0.40$
	Infrared	$0.16 \pm 0.12$ (12)	$0.29 \pm 0.11$ (12)	$0.32 \pm 0.12$ (12)	$0.27 \pm 0.11$ (12)	...
	ASPCAP	...	...	...	...	...

<sup>a</sup>  $[X/H]$  is given for Fe I instead.

<sup>b</sup> For elements where  $N < 5$  and  $\sigma$  is less than  $\sigma_{\text{FeI}}$ , the error is reported as  $\pm \sigma_{\text{FeI}}/\sqrt{N}$ ; this is also applied to Tables 8 and 9.

<sup>c</sup> A \* indicates the case where there was a synthetic fit to molecular bands of  $^{12}\text{C}^{16}\text{O}$  and  $^{12}\text{C}^{14}\text{N}$ .

<sup>d</sup> All abundances ratios computed with respect to NLTE corrected Fe I.

<sup>e</sup> Average  $[\text{Fe I}/\text{H}]$  between optical and infrared (where applicable), corrected for NLTE.

**Table 8.** Derived abundances for NGC5466 and NGC5024: Elements in common between Optical and IR

Species <sup>a</sup>	Data source	Abundance ( $[X/Fe]$ ) $\pm \sigma/\sqrt{N}$ (#)				
		NGC5024-22254	NGC5024-50371	NGC5466-9951	NGC5466-1344	NGC5466-10186
Mg I	Optical	$0.16 \pm 0.27$ (3)	$0.50 \pm 0.14$ (3)	$0.24 \pm 0.14$ (3)	$0.27 \pm 0.15$ (3)	$0.32 \pm 0.13$ (3)
	Infrared	$0.23 \pm 0.12$ (3)	$0.25 \pm 0.12$ (3)	$-0.09 \pm 0.16$ (3)	$0.09 \pm 0.13$ (3)	-
Al I <sup>b</sup>	Optical	...	...	...	...	...
	Infrared	$-0.03 \pm 0.14$ (2)	$-0.18 \pm 0.21$ (2)	$0.25 \pm 0.16$ (3)	$-0.36 \pm 0.21$ (2)	...
Si I	Optical	$0.68 \pm 0.18$ (1)	$0.34 \pm 0.17$ (1)	$0.34 \pm 0.14$ (1)	$0.36 \pm 0.16$ (1)	$0.41 \pm 0.17$ (1)
	Infrared	$0.23 \pm 0.06$ (11)	$0.34 \pm 0.07$ (11)	$0.12 \pm 0.08$ (11)	$0.12 \pm 0.08$ (11)	...
Ca I	Optical	$0.31 \pm 0.11$ (14)	$0.26 \pm 0.07$ (15)	$0.17 \pm 0.08$ (17)	$0.18 \pm 0.07$ (15)	$0.19 \pm 0.07$ (14)
	Infrared	$0.23 \pm 0.19$ (2)	$0.25 \pm 0.42$ (2)	$0.12 \pm 0.31$ (2)	$0.15 \pm 0.25$ (1)	...
Ti I	Optical	$-0.14 \pm 0.09$ (17)	$-0.09 \pm 0.12$ (17)	$-0.24 \pm 0.07$ (15)	$0.12 \pm 0.11$ (16)	$0.13 \pm 0.11$ (14)
	Infrared	$0.15 \pm 0.20$ (1)	$< 0.30$	$0.15 \pm 0.28$ (2)	$< 0.40$	...

<sup>a</sup> All abundances ratios computed with respect to NLTE corrected Fe I.

<sup>b</sup> The optical Al I placeholder is included here to demonstrate this element *can* be derived from both the optical and the infrared.

larger than this spread. This star will be discussed further in Section 7.4.

The iron abundances of the individual stars in both clusters generally agree with the cluster metallicities quoted in the literature. NGC 5024 has an observed global metallicity of  $-2.10$  (Harris 1996; 2010) and the average found in this work (after NLTE correction) is  $-2.06 \pm 0.13$ , which we consider in good agreement. NGC 5466 has an observed metallicity of  $-1.98$  (Harris 1996; 2010) and the average abundance of this work (after NLTE correction) is  $-1.96 \pm 0.13$ , also in good agreement.

### 6.3.2 Carbon and Nitrogen

Carbon abundances are determined by fitting synthetic spectra to CO lines in the IR (formed by vibration-rotation lines throughout the spectral range 15570 - 16200Å) and to the atomic C I line at 16890Å. Since the C abundances are relatively low, the molecular lines suffer greatly from noise contamination as their line strengths are small. Thus, large uncertainties are shown in the final abundance. The C abundances of this work (derived from 4 of the 5 stars as there was no IR data for NGC 5466-10186) agree with both the ASPCAP results and Shetrone et al. (2010); see Table 7. The C abundances are compared with a Galactic sample in Fig. 6 and are similar to other Galactic stars at the same metallicity.

Nitrogen abundances can be found by fitting synthetic

**Table 9.** Derived abundances for NGC5466 and NGC5024: Additional elements from optical data

Species <sup>b</sup>	Correction	Abundance ( $[X/Fe]$ ) <sup>a</sup> $\pm \sigma/\sqrt{N}$ (#)				
		NGC5024-22254	NGC5024-50371	NGC5466-9951	NGC5466-1344	NGC5466-10186
Fe II	None	$-1.88 \pm 0.13$ (18)	$-1.90 \pm 0.09$ (23)	$-1.65 \pm 0.05$ (28)	$-1.84 \pm 0.10$ (18)	$-1.89 \pm 0.08$ (24)
Na I	None	$-0.38 \pm 0.11$ (3)	$-0.58 \pm 0.17$ (2)	$-0.28 \pm 0.19$ (1)	$-0.67 \pm 0.16$ (1)	$-0.65 \pm 0.12$ (2)
Na I	NLTE	$-0.38 \pm 0.11$ (3)	$-0.58 \pm 0.17$ (2)	$-0.28 \pm 0.19$ (1)	$-0.67 \pm 0.16$ (1)	$-0.65 \pm 0.12$ (2)
Sc II	None	$0.03 \pm 0.14$ (5)	$0.33 \pm 0.14$ (4)	$-0.01 \pm 0.08$ (6)	$0.19 \pm 0.17$ (5)	$-0.01 \pm 0.11$ (3)
Ti II	None	$0.52 \pm 0.09$ (17)	$0.56 \pm 0.10$ (20)	$0.29 \pm 0.09$ (34)	$0.37 \pm 0.09$ (18)	$0.40 \pm 0.07$ (23)
V I	None	$0.07 \pm 0.14$ (5)	$0.27 \pm 0.17$ (1)	$-0.10 \pm 0.19$ (1)	...	$0.41 \pm 0.17$ (1)
V I	HFS	$0.14 \pm 0.09$ (5)	$0.22 \pm 0.17$ (1)	$-0.17 \pm 0.19$ (1)	...	$0.34 \pm 0.17$ (1)
Cr I	None	$-0.79 \pm 0.33$ (5)	$-0.33 \pm 0.11$ (3)	$-0.34 \pm 0.17$ (5)	$-0.18 \pm 0.10$ (3)	$-0.27 \pm 0.11$ (3)
Cr I	NLTE	$-0.57 \pm 0.32$ (5)	$-0.11 \pm 0.11$ (3)	$-0.12 \pm 0.17$ (5)	$0.04 \pm 0.10$ (3)	$-0.05 \pm 0.11$ (3)
Cr II	None	$0.50 \pm 0.25$ (3)	$0.32 \pm 0.25$ (3)	$0.55 \pm 0.15$ (4)	$0.36 \pm 0.18$ (3)	$0.17 \pm 0.11$ (4)
Cr II	NLTE	$0.55 \pm 0.25$ (3)	$0.37 \pm 0.25$ (3)	$0.59 \pm 0.15$ (4)	$0.40 \pm 0.18$ (3)	$0.22 \pm 0.11$ (4)
Mn I	None	$-0.21 \pm 0.13$ (2)	$-0.59 \pm 0.15$ (5)	$-0.26 \pm 0.20$ (6)	$-0.68 \pm 0.09$ (4)	$-0.58 \pm 0.11$ (3)
Mn I	HFS	$-0.39 \pm 0.13$ (2)	$-0.65 \pm 0.14$ (5)	$-0.36 \pm 0.20$ (6)	$-0.24 \pm 0.09$ (4)	$-0.52 \pm 0.11$ (3)
Co I	None	$0.02 \pm 0.33$ (2)	...	$-0.38 \pm 0.19$ (1)	$-0.22 \pm 0.16$ (1)	...
Ni I	None	$-0.31 \pm 0.20$ (6)	$-0.14 \pm 0.09$ (6)	$0.00 \pm 0.21$ (8)	$-0.18 \pm 0.09$ (7)	$-0.05 \pm 0.13$ (5)
Cu I	None	...	$-0.52 \pm 0.17$ (1)	...	...	...
Zn I	None	$0.25 \pm 0.18$ (1)	$0.30 \pm 0.17$ (1)	$-0.33 \pm 0.19$ (1)	$-0.07 \pm 0.16$ (1)	$0.01 \pm 0.17$ (1)
Y II	None	$0.00 \pm 0.21$ (4)	$-0.11 \pm 0.13$ (4)	$-0.43 \pm 0.12$ (3)	$-0.48 \pm 0.10$ (3)	$-0.36 \pm 0.11$ (3)
Ba II	None	$0.17 \pm 0.28$ (4)	$0.25 \pm 0.09$ (4)	$0.02 \pm 0.24$ (5)	$0.04 \pm 0.09$ (3)	$0.11 \pm 0.14$ (4)
La II	None	$0.63 \pm 0.15$ (2)	$0.52 \pm 0.17$ (1)	$0.56 \pm 0.19$ (1)	...	...
Nd II	None	$0.16 \pm 0.21$ (2)	$0.11 \pm 0.17$ (1)	$0.09 \pm 0.14$ (2)	$0.21 \pm 0.16$ (1)	$0.18 \pm 0.12$ (2)
Eu II	None	...	$0.74 \pm 0.17$ (1)	$0.71 \pm 0.19$ (1)	...	$0.70 \pm 0.17$ (1)

<sup>a</sup>  $[X/H]$  is given for Fe II instead.

<sup>b</sup> All abundances ratios computed with respect to NLTE corrected Fe I.

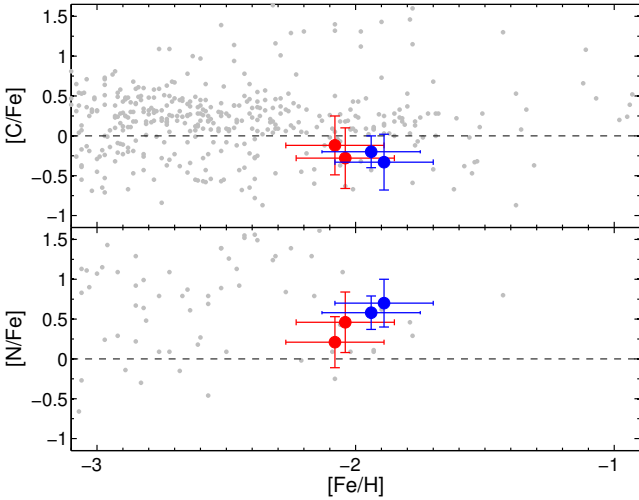


**Figure 6.** C and N abundances of stars in NGC 5024 and NGC 5466 plotted as a function of Fe I, compared with Galactic stars from Frebel (2010b) and Reddy et al. (2006) (grey points). Red and blue circles represent NGC 5024 and NGC 5466 stars, respectively.

spectra to the CN electronic transition lines located through the IR spectral range 15200 - 15600Å. The abundances must be determined *after* the C and O abundances are set (refer to section 5) because of the C dependence of the molecular lines. The derived N abundances agree with the ASPCAP values (Table 7) and are consistent with Galactic stars of

similar metallicity (see Fig. 6). Similar to C, the somewhat large uncertainty is due to relatively weak CN lines suffering from noise contamination.

### 6.3.3 $\alpha$ -elements

Alpha elements (O, Mg, Si, and Ca) are constructed via the capture of  $\alpha$  particles ( $^4\text{He}$  nuclei) during the hydrostatic burning phase of massive stars and  $\alpha$ -rich explosive nucleosynthesis during Type II supernovae (SN II). Ti is also included as an alpha element as it resembles the other alpha elements in the distribution of  $[\alpha/Fe]$  ratios in Galactic metal-poor field stars. Comparing the alpha elements to Fe (which dominates the yields from Type Ia SN) then the  $[\alpha/Fe]$  ratios can inform us on the relative contributions from each type of supernova to the interstellar medium.

*Oxygen:* O abundances are derived from both the optical and the IR. The only line measured in the optical is the forbidden line (6300 Å, generally quite weak, spanning  $13 < EW < 32$  Å) while O derived from the IR comes from  $\sim 12$  OH vibration-rotation lines spanning the spectral range 15260 - 16710 Å. The O abundance derived in 5466-10186 is an upper limit determined from spectrum synthesis. The derived optical and IR O abundances are discrepant (see Table 7), which is not uncommon (e.g., see Israelian et al. 2004; García Pérez et al. 2006). The discrepancy is partially due to a Ni I blend with the forbidden O I line in the optical and that there are a small number of optical O I lines compared to the numerous IR OH lines. Also, large systematic effects are found for the OH lines due to temperature uncertainties

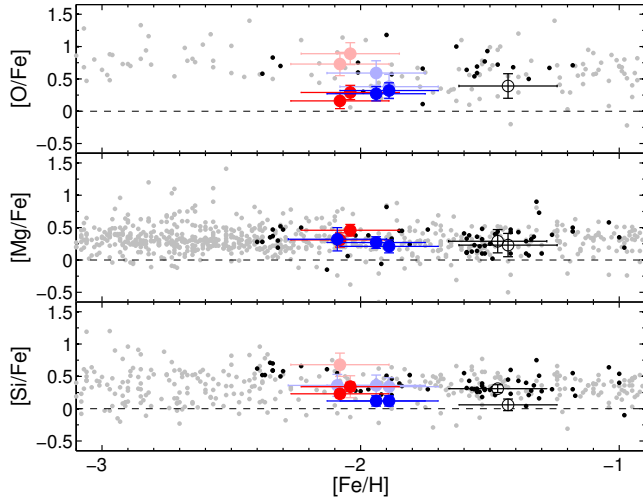


**Figure 7.** O, Mg, and Si alpha element abundances of stars in NGC 5024/5466 plotted as a function of Fe I, compared with Galactic stars from the literature. Red circles represent NGC 5024 stars while blue circles are those of NGC 5466 - O and Si abundances come from IR measurements while Mg abundances come from a weighted average between optical and IR (see text). Light gray points represent Galactic distributions of field stars summarized by Venn et al. (2004), Frebel (2010b), and Reddy et al. (2006). Black points represent Galactic GCs, assembled by Pritzl et al. (2005). The hollow black points are abundances derived from the standard stars in M3 and M13. The transparent points in the O and Si plots are abundances derived in the optical where only 1 line was available for abundance determination (one transparent point is hidden behind its infrared data point in the Si plot and there is one additional transparent Si point as there is no IR data for that star).

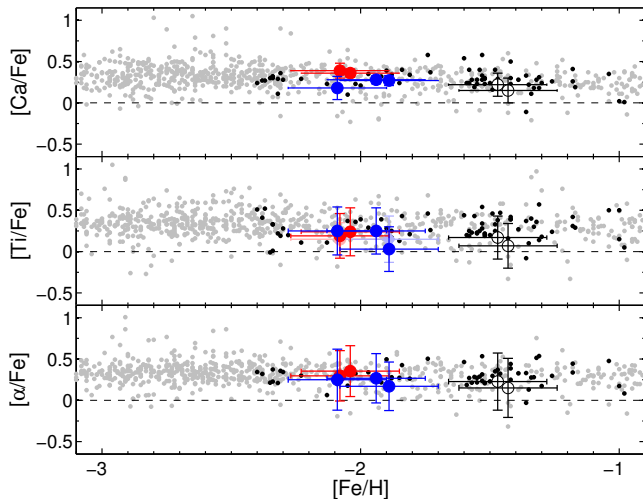


**Figure 8.** Ca, Ti, and  $\alpha$  abundances of stars in NGC 5024/5466 plotted as a function of Fe I, compared with Galactic stars from the literature as described in Fig. 7. Only the optical Ti abundance is included, and it is computed as a weighted average between TiI and TiII.

**Table 6.** Standard star abundance comparison

M3-C41303-2217 comparison with CM05						
Species <sup>a</sup>	Abundance	$\sigma$	N	Abundance	$\sigma$	N
	This work			CM05		
[Fe I/H]	-1.33	0.05	103	-1.37	0.05	126
[Fe II/H]	-1.33	0.05	14	-1.34	0.05	14
[O/Fe]	0.49	0.10	2	0.33	0.05	2
[Na/Fe]	-0.27	0.05	2	-0.39	0.09	3
[Mg/Fe]	0.33	0.13	2	0.40	0.11	3
[Al/Fe]	0.32	0.20	2	...	...	...
[Si/Fe]	0.16	0.08	2	0.20	0.05	9
[Ca/Fe]	0.25	0.05	16	0.08	0.05	15
[Sc/Fe]	-0.01	0.05	3	0.15	0.05	7
[Ti/Fe]	0.17	0.05	29	0.10	0.05	25
[V/Fe]	0.05	0.10	12	-0.18	0.06	8
[Cr/Fe]	0.08	0.05	7	0.01	0.06	9
[Mn/Fe]	-0.25	0.13	6	-0.27	0.14	4
[Co/Fe]	0.10	0.30	2	-0.11	0.03	3
[Ni/Fe]	0.03	0.08	16	-0.16	0.05	15
[Cu/Fe]	-0.44	0.09	3	-0.56	0.21	2
[Zn/Fe]	0.24	0.08	2	-0.10	0.05	2
[Y/Fe]	-0.21	0.08	4	-0.15	0.10	4
[Ba/Fe]	0.12	0.08	4	0.16	0.05	3
[La/Fe]	0.23	0.05	3	-0.02	0.15	2
[Nd/Fe]	0.25	0.07	4	0.28	0.06	5
[Eu/Fe]	0.65	0.10	1	0.51	0.10	1

mean  $\pm$  st. dev.  $\bar{\Delta} = 0.08 \pm 0.13$

M13-III-18 comparison with CM05						
[Fe I/H]	-1.57	0.05	118	-1.43	0.05	123
[Fe II/H]	-1.34	0.05	23	-1.46	0.05	13
[O/Fe]	...	...	...	0.35	0.10	1
[Na/Fe]	0.57	0.08	4	0.36	0.06	4
[Mg/Fe]	0.39	0.13	3	0.29	0.14	3
[Al/Fe]	1.07	0.06	2	0.74	0.10	1
[Si/Fe]	0.41	0.05	6	0.36	0.05	13
[Ca/Fe]	0.32	0.05	15	0.10	0.05	13
[Sc/Fe]	0.31	0.20	5	0.21	0.05	7
[Ti/Fe]	0.27	0.05	46	0.09	0.05	22
[V/Fe]	0.04	0.07	11	-0.11	0.05	8
[Cr/Fe]	0.11	0.07	8	-0.01	0.05	7
[Mn/Fe]	-0.25	0.09	7	-0.25	0.08	4
[Co/Fe]	0.16	0.27	2	-0.02	0.06	4
[Ni/Fe]	0.08	0.05	11	-0.09	0.05	18
[Cu/Fe]	-0.45	0.08	3	-0.61	0.13	2
[Zn/Fe]	0.09	0.10	1	-0.05	0.05	2
[Y/Fe]	0.01	0.09	5	-0.26	0.06	5
[Ba/Fe]	0.39	0.05	4	0.36	0.05	3
[La/Fe]	0.41	0.06	4	0.09	0.09	3
[Nd/Fe]	0.40	0.05	3	0.31	0.06	7
[Eu/Fe]	0.70	0.10	1	0.58	0.10	1

mean  $\pm$  st. dev.  $\bar{\Delta} = 0.14 \pm 0.11$

<sup>a</sup> A line weighted average is calculated for species with more than one ionization state to stay consistent with CM05. The [Ab/Fe] is calculated with respect to Fe I except for with O which is calculated with Fe II to match CM05.

<sup>b</sup>  $\Delta = (\text{This Work} - \text{CM05})$

in model atmospheres (García Pérez et al. 2006, 2013), and 3D and NLTE effects are not expected to have a major effect on the optical forbidden line (Kiselman 1993; García Pérez et al. 2006), but may play a role in the line formation of the infrared OH lines. Smith et al. (2013) have reproduced the optical abundances from IR spectra of several nearby field

giants using 1D and LTE atmospheres in the same spectral windows and line lists used here. In this paper, the IR measurements are adopted for oxygen, as shown in Fig. 7.

*Magnesium:* Mg abundances are derived from both the optical and IR spectra. The optical abundances are mostly determined from three MgI lines at 4703, 5528, and 5711 Å; the first two lines are generally strong ( $100 < EW < 140$  mÅ) and the third is generally weak ( $EW \sim 40$  mÅ) while the IR abundances are determined from the three strong lines ( $EW > 140$  mÅ) at 15740, 15748, and 15765 Å. A weighted average between the optical and IR abundances is computed and shown in Fig. 7: the resulting abundances agree with most of the other Galactic stars at the same metallicity.

*Silicon:* Only a single weak Si line ( $EW \sim 20$  mÅ) is available in the optical (at 6155 Å) and is not in very good agreement with the IR Si abundance (see Table 8). Therefore the final reported Si abundance is only from the  $\sim 11$  lines found in the IR (spanning 15370-16380 Å, where the lines have varied strength). Fig. 7 shows that the four target stars (those with IR spectra) have Si abundances which are consistent with other Galactic stars at the same metallicity.

*Calcium:* Ca abundances are determined from both optical and IR lines. Although there are significantly more available lines in the optical ( $\sim 15$ , found over the spectral range 5588-6717 Å, of varied strength) than compared with the IR (2 relatively weak features at 16150 and 16196 Å) the abundances are found to be in good agreement (see Table 8). The weighted average abundance between the two wavelength regions (computed when both data sets are available) shows Ca in the target stars is comparable to other stars in the Galactic sample at roughly the same metallicity (see Fig. 8).

*Titanium:* There are numerous TiI and TiII lines available in the optical, spanning the entire wavelength range and of varied line strength; conversely there are very few lines in the IR. Final Ti abundances are determined from the average between TiI and TiII lines (30-40) in the optical while the single TiI line in the IR (at 15335 Å) is omitted as it may be less reliable due to line blending with Fe I. The errors from the abundances of both ionization states are added in quadrature and reported here. Table 8 indicates the IR Ti abundances are in excellent agreement with the optical. Fig. 8 reveals the Ti in the target stars behaves in a similar manner to stars of similar metallicity in the Milky Way. The abundance discrepancy found between Ti I and Ti II (typically  $\sim 0.2$  dex) is a feature which is seen in other work (Letarte et al. 2010; Lemasle et al. 2012), but not found here. This discrepancy could be explained by NLTE effects associated with Ti I, described by Bergemann (2011). However the stellar parameters were outside the range of the target stars in this work and so NLTE corrections are not applied.

*Alpha:* In this work, an  $\alpha$ -element abundance is defined as the average of Ca, Mg, and Ti, and is calculated for both the target stars and Galactic distributions taken from the literature. The results are shown in Fig. 8. Results for the target stars are consistent with the Galactic distribution. Ca and Mg abundances are derived from both optical and infrared data, and their weighted averages are shown here. Ti is reported here as the average between Ti I and Ti II, and their respective errors are added in quadrature.

*Sodium and Aluminum:* Sodium abundances are derived in the optical from the D1 and D2 lines (if the D lines are

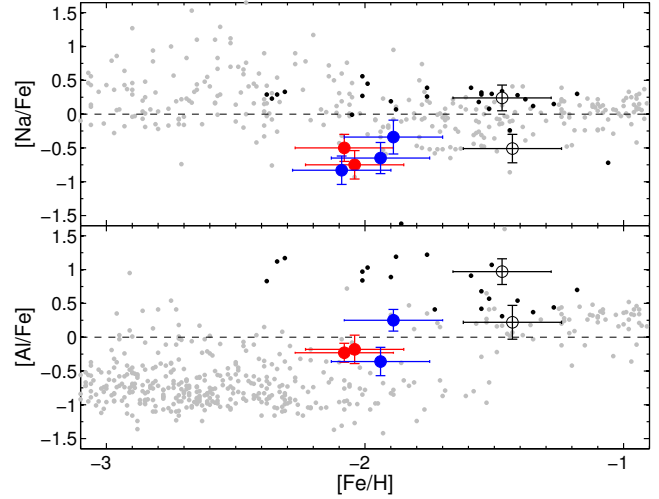


**Figure 9.** Na and Al abundances of stars in NGC 5024/5466 plotted as a function of Fe I, compared with Galactic stars from the literature as described in Fig. 7. The Na abundances in the literature are reported with or without NLTE corrections, depending on the source. Na abundances for our target stars were determined from optical data (with NLTE corrections) while the Al abundances are from infrared data (explaining why there are only 4 data points).

the only available measurements then lines above 200 mÅ are kept) and the line at 5688 Å (which is generally weak,  $\sim 20$  mÅ). Sodium is known to have a range of NLTE effects that are line dependent, but also depend on the Fe and  $T_{\text{eff}}$  of the models. Corrections have been applied following Lind et al. (2011)<sup>10</sup>, where NLTE corrections ranged from -0.05 dex (for the 5688 Å line) up to -0.29 for the D lines. Abundance measurements are shown in Fig. 9, almost all of which are relatively low compared to the Galactic GCs. The GC abundance average would include the second-generation Na-enhanced stars.

Aluminum lines were only found in the higher metallicity standard stars at optical wavelengths. Conversely, there are three strong ( $EW > 100$  mÅ) Al I lines in the IR at 16718, 16750, and 16760 Å. The Galactic distribution of Al in stars around this metallicity is quite dispersed and the NGC 5466/5024 stars fall more or less within the Galactic field star distribution.

#### 6.3.4 Iron-peak Elements

*Scandium, vanadium, and manganese* are derived exclusively from optical data, using 1-6 spectral lines (per element) and are shown in Fig. 10. Scandium is found entirely from singly ionized lines and two of the five target stars have slightly high Sc abundances. As noted in Section 6, HFS corrections were negligible for Sc. V was derived for two stars from each target cluster from generally weak lines ( $EW \sim 20$  mÅ). Hyperfine structure corrections for V were calculated and applied to each individual star (typically -0.07 dex, following the references discussed in Section 6). The V abundance appears consistent with the Galactic sample although there

<sup>10</sup> Adopted from the online database at <http://inspect-stars.net/>

is a significant scatter in V for the NGC 5466 stars; these NGC 5466 abundances are measured from a single V line in each star and the scatter agrees within the errors therefore this scatter may not be real. The Mn lines varied in strength and were found to have significant hyperfine structure corrections (ranging from -0.06 to -0.21 dex, depending on the star); after applying these corrections (again following the references in Section 6) the Mn in the target stars appears to follow the Galactic distribution at their respective metallicities. Bergemann & Gehren (2008) show that a metal-poor star ( $[\text{Fe}/\text{H}] \sim -2.5$ ) with similar stellar parameters to the targets in this work and has a *total* NLTE correction of +0.44 dex, however there are no stars in their sample that share the same parameter space as our standard stars. We do not apply this correction because this would not allow a comparison with our standard stars and it is unclear whether the correction of Bergemann & Gehren (2008) applies to the same lines of this work. However, it should be noted that NLTE effects are strong for Mn lines within the stellar parameters of our sample.

*Chromium, cobalt, and nickel* are also derived exclusively in the optical. The Cr abundance is reported as a line weighted average between 6-10 Cr I and Cr II lines found over the spectral range 4550-6330 Å and of varying line strength. The discrepancy between Cr I and Cr II is apparent, which can be attributed to NLTE effects of Cr I, e.g. Bergemann & Cescutti (2010b). NLTE corrections were found by locating stars of a similar metallicity to this sample, looking at common chromium lines between the two datasets, and then extracting the NLTE abundance correction. The NLTE correction was applied line by line to the abundances in this sample, with corrections typically found to be 0.22 dex for target stars and 0.10 dex for the standard stars; the Cr II correction also applied in the same manner and was generally found to be much smaller ( $\sim 0.05$  dex). The Cr abundance in the NGC 5024/5466 stars is slightly higher than the Galactic distribution (see Fig. 11), however given the NLTE corrections and 1- $\sigma$  uncertainties then we consider our results in good agreement with the other Galactic globular cluster data. Co is found in both cluster stars from weak lines ( $\text{EW} \sim 20$  mÅ). In NGC 5024 Co is found in one of the stars, specifically from 2 lines at 5483 and 5647 Å and agrees with the Galactic distribution (see Fig. 11). In both the NGC 5466 stars Co is determined from 1 line at 5483 Å. Bergemann et al. (2010a) find Co NLTE corrections for the same star used to find Mn NLTE corrections in Bergemann & Gehren (2008). They find Co has high NLTE corrections at low metallicities, similar to Mn, and find corrections of 0.64 dex for the star that shares the same parameter space with this work. Co NLTE corrections are not applied to this work for the same reasons discussed with Mn. Finally, Ni abundances are derived from 5-8 optical lines of varied strength and are in good agreement with other Galactic stars at this metallicity.

### 6.3.5 Copper and Zinc

*Copper and zinc* measurements are relatively scarce in the literature, thus an additional source is added (Mishenina et al. 2002) for comparison. Copper is only detected in one of the NGC 5024 stars (from the single weak line at 5105 Å) and not in NGC 5466. Zinc is measured in all the tar-

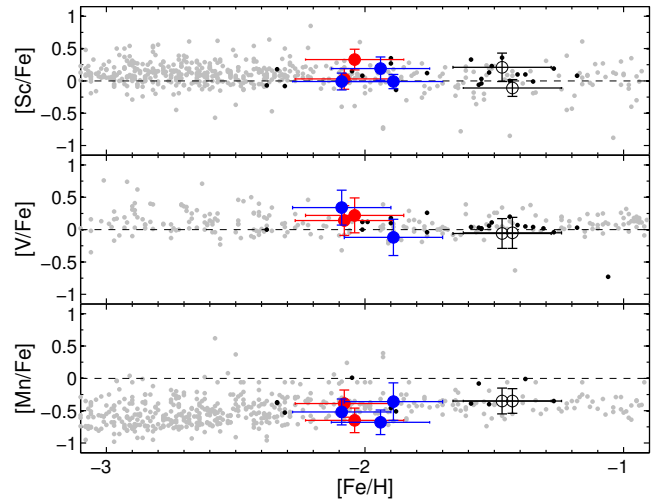


**Figure 10.** Sc, V, and Mn abundances of stars in NGC 5024/5466 plotted as a function of Fe I, compared with Galactic stars from the literature as described in Fig. 7.

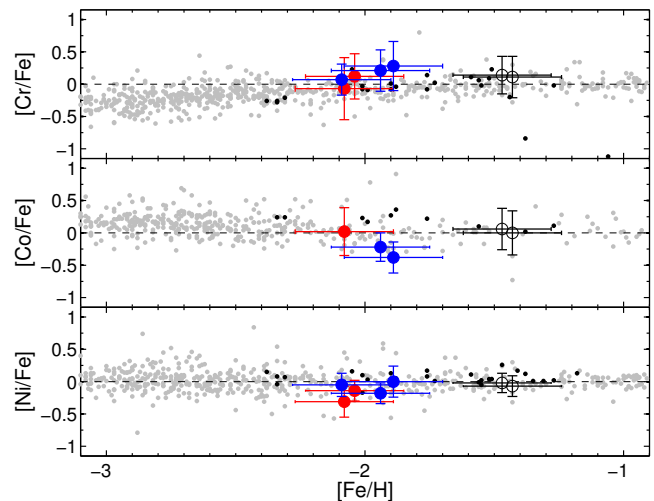


**Figure 11.** Cr, Co, and Ni abundances of stars in NGC 5024/5466 plotted as a function of Fe I, compared with Galactic stars from the literature as described in Fig. 7. The Cr abundance is reported as a weighted average between Cr I and Cr II, where NLTE corrections have been applied to each ionization state.

get stars from the neutral line at 4722 Å (typically with an EW of 40 mÅ); the NGC 5466 stars show a trend slightly lower (see Fig. 12). The NGC 5466 Zn abundance was noted to be significantly low in a detailed abundance analysis of a single anomalous cepheid star reported by McCarthy & Nemeč (1997). They argue that since the low  $[\text{Zn}/\text{Fe}]$  ratio should reflect the primordial abundance of their target star and predicted other stars would also be low in Zn.

### 6.3.6 Neutron-capture Elements

The neutron-capture elements come from one of two processes: either the slow process (or s-process) via AGB stellar winds or through the rapid process (r-process) during SNe II nucleosynthesis. Burris et al. (2000) have shown that in

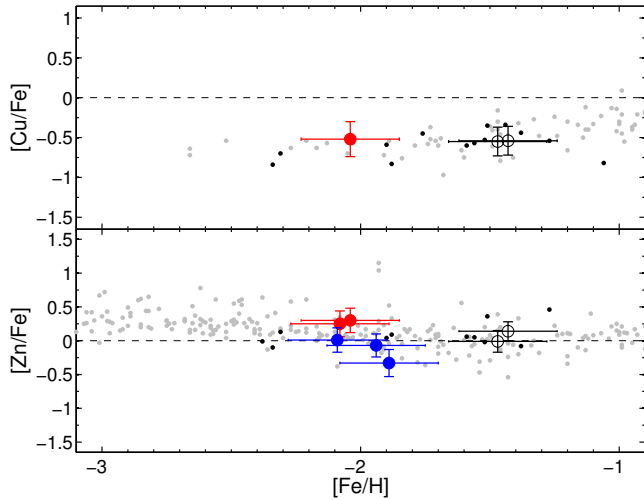


**Figure 12.** Cu and Zn abundances of stars in NGC 5024/5466 plotted as a function of Fe I, compared with Galactic stars from the literature as described in Fig. 7. Also included are Cu and Zn abundances from Mishenina et al. (2002), also plotted as light gray points. The Cu line used to compute the Cu abundance is quite weak and only detectable in NGC 5024-50371.

the Sun 97 % of the Eu abundance originates from the r-process, whereas at least 72% of the Y, Ba, and La in the Sun come from the s-process. Thus these elements are excellent indicators as to which of these two types of processes have been involved within the environment of the cluster.

*Yttrium* is detected in all five target stars from 3-4 singly ionized lines of varied strength in the optical data. Y in both clusters is consistent with the Galactic comparison sample. The abundance in the two NGC 5024 stars is higher than those in NGC 5466 (see Fig. 13). The Y can be seen to have little star to star variations within each cluster and is also in agreement with the standard stars in M3 and M13.

*Barium* is detected in all five target stars from 3-5 strong ( $EW > 100$  mÅ) singly ionized lines in the optical. Fig. 13 shows the small star to star dispersion of Ba within each cluster and it also shows the Ba is in good agreement with the M3/M13 standard stars.

*Lanthanum* is detected from only 1-2 weak, singly ionized optical lines in the NGC 5024 stars and one NGC 5466 star. These La abundances appear to be slightly higher than our M3/M13 stars and the Galactic distribution (see Fig. 13).

*Neodymium* abundances are measured from 1-2 weak lines from the optical data (at 5249 and 5319 Å) for all five of the target stars. Nd measurements show very little star to star variation within each cluster and also agree with our standard stars (see Fig. 14).

*Europium* is only detected in three stars (two in NGC 5466 and one in NGC 5024) from the weak 6645 Å line in the optical ( $EW \sim 15$  mÅ for all three stars). Fig. 14 shows the measured Eu abundance in both clusters is relatively higher than the Galactic distribution.

To validate the accuracy of the Eu abundance derived from the EW analysis we synthesize the weak line at 6645 Å for a single star (NGC 5466-9951) and compare. Fig. 15 shows a synthetic spectrum for the EW Eu abundance with

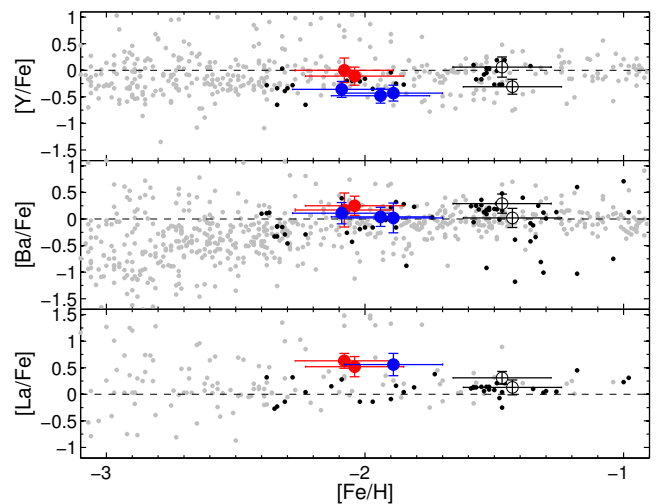


**Figure 13.** Y, Ba, and La abundances of stars in NGC 5024/5466 plotted as a function of Fe I, compared with Galactic stars from the literature as described in Fig. 7.

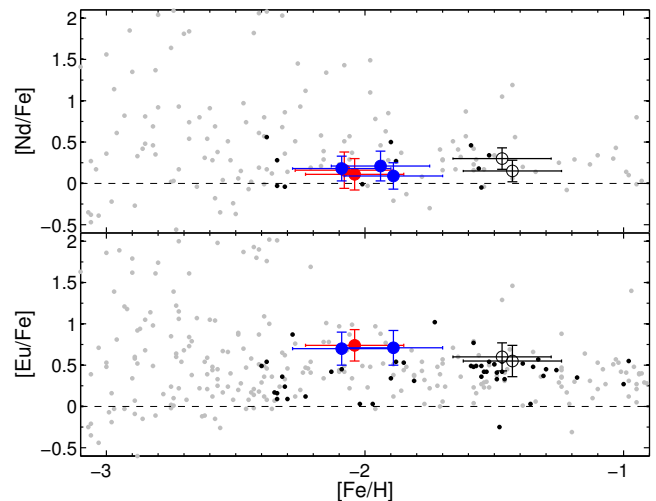


**Figure 14.** Nd and Eu abundances of stars in NGC 5024/5466 plotted as a function of Fe I, compared with Galactic stars from the literature as described in Fig. 7.

1 sigma errors. Also shown is the synthetic fit to the weak La line in the same star, where the synthetic spectrum is created with the EW La abundance (also with 1 sigma errors).

## 7 DISCUSSION

### 7.1 Infrared Abundance Comparison with Optical and Literature Abundances

There are 7 elements from the sample of stars in this work (including standard stars) which have abundances derived from both the optical and the IR: Fe, O, Mg, Al, Si, Ca, and Ti (although Al is only derived in the optical for our standard stars, it is included here to demonstrate it is among the list of elements that *can* be compared between the two wavelength analyses). Tables 7 and 8 summarize the reported abundances and show the excellent agreement of Fe derived

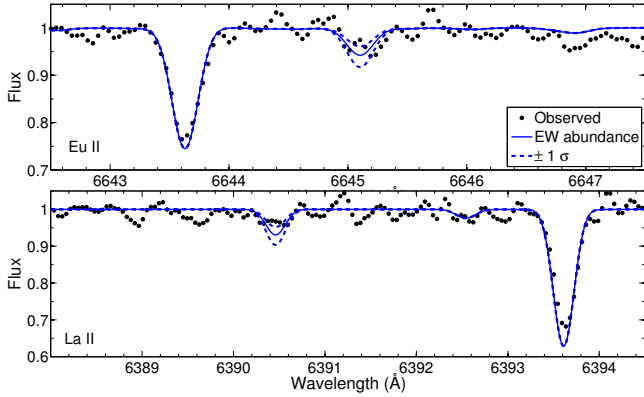


**Figure 15.** Top: synthetic abundance fit to the single Eu line in NGC 5466-9951; the 1 sigma errors here are 0.19 dex. The spectrum synthesis agrees with the EW analysis abundance. Bottom: synthetic fit to the weak La line in the same star, along with 1 sigma errors (0.19 dex); the synthetic abundance agrees with the EW abundance.

from the optical and the IR. The uncertainties shown here reflect both random and systematic errors. The ASPCAP (see Section 4.2) Fe abundances are also in excellent agreement, even though the model atmospheres used to compute the abundances in this work have different parameters (although within the errors, see Table 4). In Fig. 16, we compare the optical and IR abundance results for the remaining six elements that are found in both wavelength regions (Fe is excluded as the abundances are shown as  $[X/Fe]$ ), as well as C and N. There are reported abundances for C and N from ASPCAP and for C and N from Shetrone et al. (2010) and Martell et al. (2008). The IR C abundance in NGC 5024 is in excellent agreement with ASPCAP and Martell et al. (2008). Similarly the IR C abundance in NGC 5466 is consistent both with ASPCAP and Shetrone et al. (2010). The N abundance in both clusters also shows consistency with ASPCAP. The O abundance derived in the IR is much lower than that of the optical for the two stars in NGC 5024; this discrepancy is discussed in section 6.3.3 and we favour the IR results. The rest of the element abundances are consistent, with the exception of Si in one star; we favour the IR abundances for Si since there are only 1-2 measured lines in the optical but many more lines in the IR.

## 7.2 r and s-process Contributions

Europium is used as a proxy for the r-process (based on an analysis of the solar system distribution of the heavy elements, e.g., Arlandini et al. 1999; Burris et al. 2000), whereas Y, La, and Ba are formed in a number of nucleosynthetic sites ranging from core collapse SN to the s-process during the thermal pulsing in AGB stars. Gallino et al. (1990) and Busso et al. (1999) showed that the s-process yields in AGB stars are metallicity dependent, such that low metallicity AGB stars will bypass the first s-process peak elements in favour of the second and third peak elements due to a lack of iron seed nuclei. In Galactic field stars, the increase in these elements from the s-process can be seen between metallicities of  $-3 < [Fe/H] < -2$  (e.g., McWilliam et al. 1995; McWilliam 1998). Fig. 17 shows  $[Ba/Eu]$  and  $[Ba/Y]$

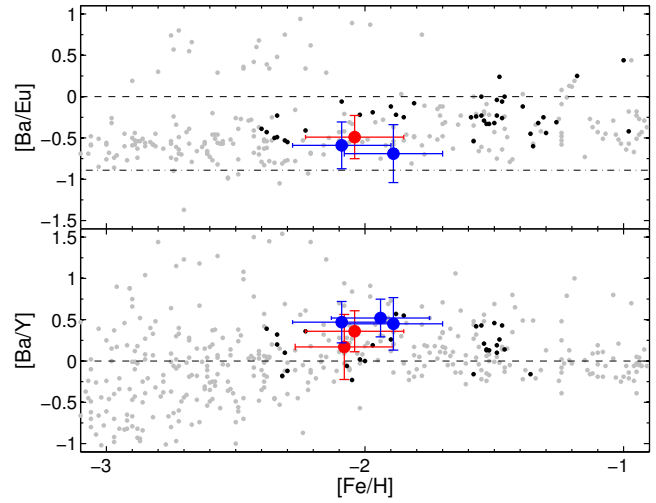


**Figure 17.**  $[Ba/Eu]$  vs  $[Fe/H]$  and  $[Ba/Y]$  for the NGC 5024/5466 stars with available abundances. The lower dashed-dotted line in the top plot represents the lowest  $[Ba/Eu]$  ratio possible, where only the r-process contributes to these elements (Burris et al. 2000).

as a function of metallicity in Galactic globular clusters and field stars; the r-process yield in  $[Ba/Eu]$  from Burris et al. (2000) is also shown. The slightly elevated  $[Ba/Eu]$  values in our two globular clusters are consistent with a mild s-process contribution, and the  $[Ba/Y]$  values suggest those contributions are from metal poor AGB stars.

## 7.3 Evidence for Mixing

The locations of the target stars on their colour-magnitude diagrams (CMDs) are shown in Fig. 18; photometry is from Sarajedini et al. (2007); Anderson et al. (2008). All of our targets are bright stars located near the tip of the red giant branch, above the RGB bump, where mixing of CNO-cycled H-burning gas is expected (e.g., Suntzeff & Smith 1991; Smith & Martell 2003; Smith & Briley 2006; Charbonnel et al. 1998; Sweigart & Mengel 1979; Charbonnel 1995; Bellman et al. 2001; Denissenkov & Vandenberg 2003; Carretta et al. 2005). This will have the effect of elevated N (by  $\sim 0.5$  dex), slightly depleted C (by  $\sim 0.2$  dex), and even slighter depletions of oxygen ( $< 0.1$  dex) from their initial abundances (Carretta et al. 2005). Assuming the globular clusters started with solar C and N, then the  $[(C+N)/Fe]$  abundances will remain  $\sim$ solar (we ignore the very small change in oxygen that is expected from its enhanced, Galactic plateau, initial value). The  $[(C+N)/Fe]$  values are shown in Fig. 19, and are consistent with standard mixing as the sums remain near solar. NGC5466-9951 also shows slight enhancements in Na and Al suggestive of primordial variations or pollution within the cluster (e.g., Gratton et al. 2004; Carretta et al. 2009). This suggests that NGC 5466-9951 may be a member of a second generation population in this cluster.

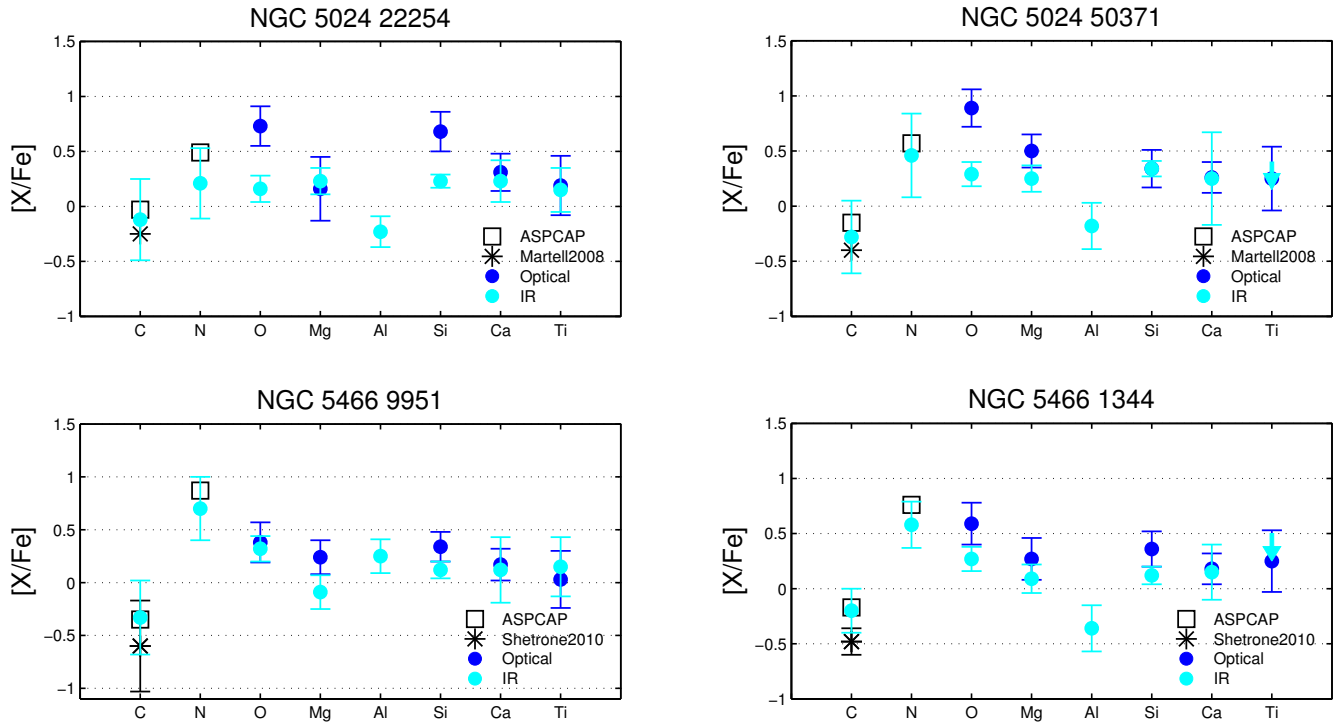


**Figure 16.** Abundance comparison of overlapping elements between target stars. The blue points are from the optical observations of this work, the cyan points from infrared APOGEE observations, the square points from APOGEE’s abundance pipeline ASPCAP, and the asterisk points from Martell et al. (2008) (NGC 5024), Shetrone et al. (2010) (NGC 5466). The errors reported here reflect both random and systematic uncertainties. The ASPCAP points and the points of Martell et al. (2008) are plotted without errors, as the reported values in each case are negligibly small and perhaps do not reflect the true spread in the measurements. In general, the results are consistent except for O and Si in NGC 5024-22254 and for O in NGC 5024-50371.

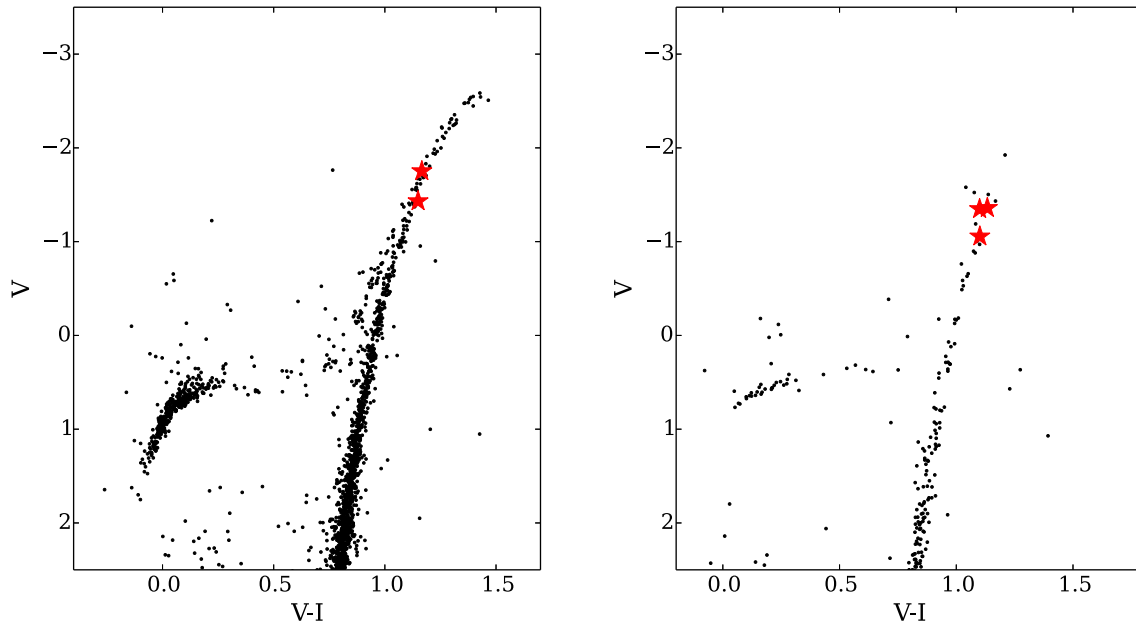


**Figure 18.** Colour-magnitude diagrams for the globular clusters NGC 5024 (left) and NGC 5466 (right), with photometry taken from the ACS Survey of Galactic Globular Clusters (Sarajedini et al. 2007; Anderson et al. 2008). The symbols in red are the target stars from this work.

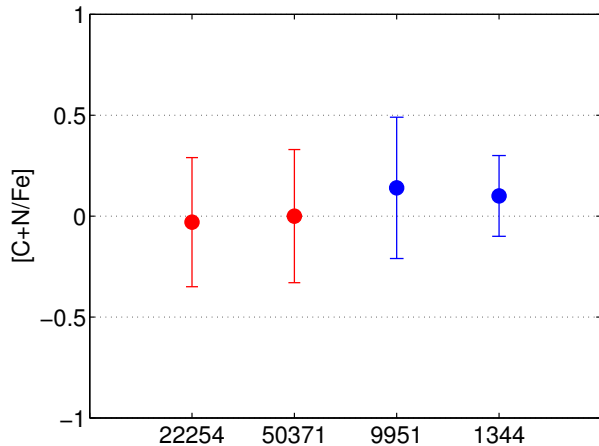


**Figure 19.** [C+N/Fe] abundances to the NGC 5024/5466 stars where the data was available. The red and blue points are those of NGC 5024 and NGC 5466, respectively.

#### 7.4 NGC 5024/5466 /origins

NGC 5024 and NGC 5466 do not show any distinct abundance differences with GC and field stars within the MW, although at these low metallicities it is difficult to discern whether the abundances of these clusters would show extragalactic signatures. As previously described, this is because at low metallicities GCs like M54 do not show chemical abundance patterns that stand out with GCs in the MW, even though it has physical associations with a dwarf remnant. However, M54 and  $\omega$  Cen *do* show an Fe metallicity spread (i.e. 0.19 dex rms scatter for M54), and are among the few GCs known to show such a spread Carretta et al. (2010); where it is also argued this spread could be caused by large and repeated bursts of star formation. Interestingly, NGC 5466 also shows a spread in Fe abundance found from the three stars in this work (0.09 dex rms scatter from the random errors; if one considers systematics then the scatter is smaller than this value). The velocity dispersion is relatively large in this sample (12 km/s), which is also seen to be large by Shetrone et al. (2010) (17 km/s, although from low resolution spectra). It is possible that the one star NGC 5466-10186 that causes most of this velocity dispersion is a non-member, however the position of this star on the CMD and lack of foreground contamination towards this cluster makes this unlikely. It is also possible that NGC 5466-10186 is in a binary system which may have affected its apparent radial velocity and could also explain the slightly lower metallicity we have found if the binary companion has artificially increased its continuum flux levels. Before interpreting the velocity and Fe dispersions in NGC5466 in terms of its origins or physical mass, more stars should be examined in this cluster.

## 8 SUMMARY AND CONCLUSIONS

A detailed chemical abundance analysis has been performed for two RGB stars in NGC 5024 and three RGB stars in NGC 5466. In this analysis, we have found:

- (i) The optical and infrared abundances are in good

agreement for the elements Fe, Mg, Si, Ca, and Ti. There is a discrepancy in the oxygen abundances, which has been seen before in the literature. We favour our IR oxygen abundances, determined from several OH features.

- (ii) The neutron-capture elements are mildly enriched in s-process yields from metal-poor AGB stars.

- (iii) The stars in both clusters exhibit CNO mixing, as evidenced from the enhanced N, depleted C, and solar [(C+N)/Fe] ratios. One star NGC5466-9951 shows slight enhancements in Na and Al as well, which suggests it may be a member of a second generation population.

- (iv) Both globular clusters show element ratios that are similar to other Galactic clusters at this metallicity, however NGC5466 may have a larger spread in the iron abundances and a larger velocity distribution. This may be due to one star (NGC5466-10186) in a binary system, or it may represent a physical property of this cluster. Other clusters with metallicity and velocity dispersions include Omega Cen and M54, both accreted from the Sgr dwarf galaxy.

We conclude that abundances derived from both the optical and infrared regions complement each other in a stellar atmospheres analysis, and that NGC5024 and NGC5466 appear to be similar to the majority of Galactic globular clusters. Further spectroscopic analysis of NGC5466 is needed to confirm its apparent metallicity and velocity dispersions.

We are grateful to the SDSS APOGEE team for making their spectra available in addition to their ASPCAP stellar pipeline results. MPL and KAV acknowledge funding from an NSERC Discovery Grant, and CMS would like to thank NSERC for a Vanier Graduate Fellowship.

## REFERENCES

- Allen, C., Moreno, E., & Pichardo, B. 2006, ApJ, 652, 1150  
 Alonso, A., Arribas, S., & Martínez-Roger, C., 1999, A&AS, 140, 261  
 Anderson, J., Sarajedini, A., Bedin, L. R., et al. 2008, AJ, 135, 2055  
 Aoki, W., Beers, T. C., Christlieb, N., et al. 2007, ApJ, 655, 492  
 Arlandini, C., Käppeler, F., Wisshak, K., et al. 1999, ApJ, 525, 886  
 Asplund, M., Grevesse, N., Sauval, A. J., & Scott, P. 2009, ARA&A, 47, 481  
 Battaglia, G., Irwin, M., Tolstoy, E., et al. 2008, MNRAS, 383, 183  
 Bellazzini, M., Ferraro, F. R., & Ibata, R. 2003, AJ, 125, 188  
 Bellman, S., Briley, M. M., Smith, G. H., & Claver, C. F. 2001, PASP, 113, 326  
 Bergemann, M., & Gehren, T. 2008, A&A, 492, 823  
 Bergemann, M., Pickering, J., & Gehren, T. 2010, MNRAS, 401, 1334  
 Bergemann, M., & Cescutti, G. 2010, A&A, 522, A9  
 Bergemann, M. 2011, MNRAS, 413, 2184  
 Bergemann, M., Lind, K., Collet, R., Magic, Z., & Asplund, M. 2012, MNRAS, 427, 27  
 Biehl, D. 1976, Ph.D. Thesis

- Booth, A. J., Shallis, M. J., & Wells, M. 1983, MNRAS, 205, 191
- Burris, D. L., Pilachowski, C. A., Armandroff, T. E., et al. 2000, ApJ, 544, 302
- Busso, M., Gallino, R., & Wasserburg, G. J. 1999, ARA&A, 37, 239
- Busso, M., Gallino, R., Lambert, D. L., Travaglio, C., & Smith, V. V. 2001, ApJ, 557, 802
- Carretta, E., Gratton, R. G., Lucatello, S., Bragaglia, A., & Bonifacio, P. 2005, A&A, 433, 597
- Carretta, E., Bragaglia, A., Gratton, R. G., et al. 2009, A&A, 505, 117
- Carretta, E., Bragaglia, A., Gratton, R. G., et al. 2010, A&A, 516, A55
- Cayrel, R. 1989, in The impact of very high S/N spectroscopy on stellar physics, ed. G. Cayrel de Strobel, & M. Spite (Dordrecht: Kluwer Academic Publ.), IAU Symp., 132, 345
- Cayrel, R., Depagne, E., Spite, M., et al. 2004, A&A, 416, 1117
- Charbonnel, C. 1995, ApJL, 453, L41
- Charbonnel, C., Brown, J. A., & Wallerstein, G. 1998, A&A, 332, 204
- Chun, S.-H., Kim, J.-W., Sohn, S. T., et al. 2010, AJ, 139, 606
- Cohen, J. G. 2004, AJ, 127, 1545
- Cohen J.G. & Meléndez, J., 2005, ApJ, 129, 303
- Cohen, J., Christlieb, N., McWilliam, A., et al. 2008, ApJ, 672, 320
- Cordero, M. J., Pilachowski, C. A., Johnson, C. I., et al. 2014, ApJ, 780, 94
- Da Costa, G. S., & Armandroff, T. E. 1995, AJ, 109, 2533
- Dékány, I.; Kovács, G., 2009, A&A, 507, 803
- Denissenkov, P. A., & Vandenberg, D. A. 2003, ApJ, 593, 509
- Dinescu, D. I., Majewski, S. R., Girard, T. M., & Cudworth, K. M. 2000, AJ, 120, 1892
- Dotter, A., Sarajedini, A., Anderson, J., et al. 2010, ApJ, 708, 698
- Dotter, A., Sarajedini, A., & Anderson, J. 2011, ApJ, 738, 74
- Fekadu, N., Sandquist, E.L., and Bolte, M. 2007, ApJ 663, 277
- Fellhauer, M., Evans, N. W., Belokurov, V., Wilkinson, M. I., & Gilmore, G. 2007, MNRAS, 380, 749
- Font, A. S., Johnston, K. V., Bullock, J. S., & Robertson, B. E. 2006, ApJ, 646, 886
- Forbes, D. A., & Bridges, T. 2010, MNRAS, 404, 1203
- Frebel, A., Simon, J. D., Geha, M., & Willman, B. 2010b, ApJ, 708, 560
- Frebel, A. 2010, Astronomische Nachrichten, 331, 474
- Gallino, R., Busso, M., Picchio, G., & Raiteri, C. M. 1990, Natur, 348, 298
- García Pérez, A. E., Asplund, M., Primas, F., Nissen, P. E., & Gustafsson, B. 2006, A&A, 451, 621
- García Pérez, A. E., Cunha, K., Shetrone, M., et al. 2013, ApJL, 767, L9
- Gratton, R., Sneden, C., & Carretta, E. 2004, ARAA, 42, 385
- Grillmair, C. J., & Johnson, R. 2006, ApJL, 639, L17
- Gustafsson, B., Bell, R. A., Eriksson, K., & Nordlund, A. 1975, A&A, 42, 407
- Gustafsson, B., Edvardsson, B., Eriksson, K., et al., 2008, A&A, 486, 951
- Harris, W.E. 1996, AJ, 112, 1487 (2010 edition)
- Heiter, U., & Eriksson, K. 2006, AAP, 452, 1039
- Herwig, F., Vandenberg, D. A., Navarro, J. F., Ferguson, J., & Paxton, B. 2012, ApJ, 757, 132
- Hidalgo, S. L., Aparicio, A., Skillman, E., et al. 2011, ApJ, 730, 14
- Hidalgo, S. L., Monelli, M., Aparicio, A., et al. 2013, ApJ, 778, 103
- Hill, V., François, P., Spite, M., Primas, F., & Spite, F. 2000, A&A, 364, L19
- Hill, V., in McWilliam A., Rauch M., eds, Origin and Evolution of the Elements. Carnegie Observatories, Pasadena, p. 205
- Hinkle, K., & Wallace, L. 2005, Cosmic Abundances as Records of Stellar Evolution and Nucleosynthesis, 336, 321
- Ibata, R. A., Gilmore, G., & Irwin, M. J. 1994, Nat, 370, 194
- Israelian, G., Shchukina, N., Rebolo, R., et al. 2004, A&A, 419, 1095
- Jordi, K., & Grebel, E. K. 2010, A&A, 522, A71
- Kiselman, D. 1993, AAP, 275, 269
- Kobayashi, C., Umeda, H., Nomoto, K., Tominaga, N., & Ohkubo, T. 2006, ApJ, 653, 1145
- Kopacki, G. 2000, A&A, 358, 547
- Kraft, R. P. 1994, PASP, 106, 553
- Law, D. R., & Majewski, S. R. 2010, ApJ, 718, 1128
- Lawler, J. E., Bonvallet, G., & Sneden, C. 2001a, ApJ, 556, 452
- Lawler, J. E., Wickliffe, M. E., den Hartog, E. A., & Sneden, C. 2001b, ApJ, 563, 1075
- Leaman, R., Vandenberg, D. A., & Mendel, J. T. 2013, MNRAS, 436, 122
- Lemasle, B., Hill, V., Tolstoy, E., et al. 2012, A&A, 538, A100
- Letarte, B., Chapman, S. C., Collins, M., et al. 2009, MNRAS, 400, 1472
- Letarte, B., Hill, V., Tolstoy, E., et al. 2010, A&A, 523, A17
- Lind, K., Asplund, M., Barklem, P. S., & Belyaev, A. K. 2011, A&A, 528, A103
- Lind, K., Bergemann, M., & Asplund, M. 2012, MNRAS, 427, 50
- Mackey, A. D., & van den Bergh, S. 2005, MNRAS, 360, 631
- Mateluna, R., Geisler, D., Villanova, S., et al. 2012, A&A, 548, A82
- Martínez Delgado, D., Dinescu, D. I., Zinn, R., et al. 2004, Satellites and Tidal Streams, 327, 255
- Martell, S. L., Smith, G. H., & Briley, M. M. 2008, PASP, 120, 7
- McCarthy, J. K., & Nemeč, J. M. 1997, ApJ, 482, 203
- McWilliam, A., Preston, G. W., Sneden, C., & Shectman, S. 1995, AJ, 109, 2736
- McWilliam, A. 1998, AJ, 115, 1640
- McWilliam, A., Wallerstein, G., & Mottini, M. 2013, ApJ, 778, 149
- Mészáros, S., Allende Prieto, C., Edvardsson, B., et al. 2012, AJ, 144, 120
- Mishenina, T. V., Kovtyukh, V. V., Soubiran, C., Travaglio, C., & Busso, M. 2002, A&A, 396, 189

- Mottini, M., Wallerstein, G., & McWilliam, A. 2008, *AJ*, 136, 614
- Okamoto, S., Arimoto, N., Yamada, Y., & Onodera, M. 2012, *ApJ*, 744, 96
- Pilachowski, C. A., Olszewski, E. W., & Odell, A. 1983, *PASP*, 95, 713
- Plez, B., & Lambert, D. L., 2002, *A&A*, 386, 1009
- Pritzl, B. J., Venn, K. A., & Irwin, M. 2005, *AJ*, 130, 2140
- Prochaska, J. X., Naumov, S. O., Carney, B. W., McWilliam, A., & Wolfe, A. M. 2000, *AJ*, 120, 2513
- Ramírez, I. & Meléndez, J., 2005, *ApJ*, 626, 465
- Reddy, B. E., Lambert, D. L., & Allende Prieto, C. 2006, *MNRAS*, 367, 1329
- Revaz, Y., & Jablonka, P. 2012, *A&A*, 538, A82
- Sbordone, L., Bonifacio, P., Buonanno, R., et al. 2007, *A&A*, 465, 815
- Sarajedini, A., Bedin, L. R., Chaboyer, B., et al. 2007, *AJ* 133, 1658
- Shetrone, M. D., Bolte, M., & Stetson, P. B. 1998, *AJ*, 115, 1888
- Shetrone, M. D., Côté, P., & Sargent, W. L. W. 2001, *ApJ*, 548, 592
- Shetrone, M. D., Venn, K. A., Tolstoy, E., et al. 2003, *AJ*, 125, 684
- Shetrone, M., Martell, S. L., Wilkerson, R., et al. 2010, *AJ*, 140, 1119
- Skrutskie, M. F., Cutri, R. M., Stiening, R., et al. 2006, *AJ*, 131, 1163
- Smith, G. H., & Martell, S. L. 2003, *PASP*, 115, 1211
- Smith, G. H., & Briley, M. M. 2006, *PASP*, 118, 740
- Smith, M. C., Evans, N. W., Belokurov, V., et al. 2009, *MNRAS*, 399, 1223
- Smith, V. V., Cunha, K., Shetrone, M. D., et al. 2013, *ApJ*, 765, 16
- Snedden, C., 1973, *ApJ*, 184, 839
- Snedden, C., Kraft R.P., Guhathakurta, P., Peterson, R.C., & Fulbright, J. P. , 2004, *AJ*, 127, 2162
- Stetson, P. B. 2000, *PASP*, 112, 925
- Stetson, P.B. & Pancino, E., 2008, *PASP*, 120, 1332
- Suntzeff, N. B., & Smith, V. V. 1991, *ApJ*, 381, 160
- Sweigart, A. V., & Mengel, J. G. 1979, *ApJ*, 229, 624
- Tafelmeyer, M., Jablonka, P., Hill, V., et al. 2010, *A&A*, 524, A58
- Tolstoy, E., Hill, V., & Tosi, M. 2009, *ARAA*, 47, 371
- Tull, R.G., 1998, *Proc. SPIE*, 3355, 387
- Venn, K. A., Irwin, M., Shetrone, M. D., et al. 2004, *AJ*, 128, 1177
- Venn, K. A., Shetrone, M. D., Irwin, M. J., et al. 2012, *ApJ*, 751, 102
- Villanova, S., & Geisler, D. 2011, *A&A*, 535, A31
- Villanova, S., Geisler, D., Carraro, G., Moni Bidin, C., & Muñoz, C. 2013, *ApJ*, 778, 186
- Weisz, D. R., Dolphin, A. E., Skillman, E. D., et al. 2014, *ApJ*, 789, 148